cMat

WILEY

有科出版 YOUKE PUBLISHING

MINI REVIEW OPEN ACCESS

Negative Thermal Expansion in Metastable $PbVO_3$: High-Pressure Synthesis, Advances, and Perspectives

Zhao Pan[1] | Takumi Nishikubo[2,3] | Hajime Yamamoto[4] | Xubin Ye[1] | Masaki Azuma[2,3] | Youwen Long[1,5]

[1]Beijing National Laboratory for Condensed Matter Physics, Institute of Physics, Chinese Academy of Sciences, Beijing, China | [2]Institute of Integrated Research, Institute of Science Tokyo, Yokohama, Japan | [3]Kanagawa Institute of Industrial Science and Technology (KISTEC), Ebina, Kanagawa, Japan | [4]Institute of Multidisciplinary Research for Advanced Materials, Tohoku University, Sendai, Japan | [5]Songshan Lake Materials Laboratory, Dongguan, Guangdong, China

Correspondence: Zhao Pan (zhaopan@iphy.ac.cn) | Masaki Azuma (mazuma@msl.titech.ac.jp) | Youwen Long (ywlong@iphy.ac.cn)

Received: 15 May 2025 | **Revised:** 7 July 2025 | **Accepted:** 12 August 2025

Keywords: advances and perspectives | high-pressure synthesis | negative thermal expansion | $PbVO_3$-based perovskites

ABSTRACT

Most materials expand on heating; however, some materials show the opposite trend, in which the overall volume contracts upon heating, a phenomenon known as negative thermal expansion (NTE). Materials exhibiting NTE are highly valued for their unique ability to tailor thermal expansion, especially in achieving zero thermal expansion when combined with positive thermal expansion materials. NTE functional materials illustrate the significant interplay between specific physical properties and NTE. In perovskite ferroelectric NTE materials, thermal expansion can be regulated through the interaction between ferroelectricity and NTE. The temperature-induced ferroelectric-to-paraelectric phase transition is also accompanied by unusual NTE. Inspired by these, new NTE materials can be designed and realized in polar perovskites by stabilizing their metastable structures. Indeed, NTE was successfully realized in $PbTiO_3$-type perovskite of $PbVO_3$, which shows the same tetragonal perovskite structure as $PbTiO_3$, but exhibits more pronounced tetragonal distortion. Recent progress of NTE in $PbVO_3$-based derivatives has been summarized. NTE was achieved in $PbVO_3$-based derivatives through chemical substitutions at the A-site, B-site, or anion site using a distinct high-pressure synthesis method. Despite challenges in optimizing the performance of NTE, $PbVO_3$-based perovskites provide a roadmap for discovering analogous materials such as $BiCoO_3$, $Bi(Zn_{1/2}Ti_{1/2})O_3$, and $Bi(Zn_{1/2}V_{1/1})O_3$.

1 | Introduction

1.1 | The Importance of Negative Thermal Expansion (NTE) Materials

Thermal expansion is a fundamental property of all states of matter—solids, liquids, and gases—which originates from the anharmonicity of lattice vibrations [1–6]. Anharmonicity refers to the deviation of atomic interactions from ideal Hookean behavior in lattice dynamics. The Pauli exclusion principle prevents atomic orbitals overlapping beyond a critical distance. Consequently, as the interatomic distance Δr approaches zero, the potential energy of atomic bonds increases sharply (Scheme 1). Due to the asymmetric potential well, atomic bonds expand more readily than they compress. As the temperature rises, the average interatomic distance also increases. The thermal expansion of solids is measured by the relative volume change, $\Delta V/V$, corresponding to a specific temperature change. The coefficient of thermal expansion (CTE) is defined by the Grüneisen relationship (Equation (1)), which describes the interaction between phonons and thermal expansion [5]:

$$\alpha_V = \frac{\gamma C_V K}{V}, \tag{1}$$

where α_V represents the volumetric CTE, γ denotes the Grüneisen parameter, and C_V is the specific heat at constant volume. The isothermal compressibility (K) is related to the volume (V). In typical solids, K is almost constant with respect to temperature, and the value of γ typically ranges from 1 to 3.

Thermal expansion, a fundamental property of solid materials, is characterized by the expansion of materials in response to temperature changes, as governed by natural laws. Thermal expansion issues affect diverse areas, including large structures, such as roads, railway tracks, bridges, and liquefied natural gas containers, as well as precision instruments and electronic devices, such as telescopes, standard rulers, solid-oxide fuel cells, actuators, long-distance power cable core wires, and catalysis supports [5, 7]. Modern applications demand materials with excellent physical properties and controllable thermal expansion, driven by advancements in materials science and technology. Incorporating controlled thermal expansion strategies, as demonstrated in various industrial applications, can significantly enhance the reliability and extend the lifespan of devices.

Although most natural materials show normal positive thermal expansion (PTE) upon heating, some materials exhibit abnormal contraction on heating, referred to as NTE. Identifying NTE behavior in compounds enables the development of materials with adjustable or minimal thermal expansion coefficients for targeted applications. The thermal expansion properties can be tailored by combining materials with negative and positive thermal expansion properties [8–11].

1.2 | NTE Materials

The earliest documented instance of materials contracting when heated dates back several centuries to the "density anomaly of water" [12]. In 1897, Guillaume reported the Invar effect in $Fe_{0.65}Ni_{0.35}$ alloys, initially associating it with NTE [13]. Scheel first documented thermal shrinkage in quartz and vitreous silica at low temperatures in 1907 [14, 15]. The low thermal expansion characteristics of lithium aluminum silicates were identified in 1948 [16, 17], followed by the discovery of the sodium zirconate phosphate (NZP) family in 1979 [18–20]. In the early stages, these materials were commonly described as having "low thermal expansion" or "anomalous thermal expansion" instead of being specifically classified as NTE materials. It was not until the 1990s that the term "negative thermal expansion" gained traction in scientific literature. The discovery of isotropic NTE in ZrW_2O_8 in 1996 significantly transformed the landscape of NTE research [21]. This breakthrough catalyzed a surge of interest in NTE materials, establishing them as a prominent topic within the field of solid-state chemistry. Subsequent theoretical and experimental investigations led to the development of sophisticated models that explain the unusual thermal behavior of various framework compounds. This advancement enabled the precise synthesis of novel NTE compositions and established NTE as a distinct research field.

The past 2 decades have witnessed remarkable progress in NTE materials research. The diverse requirements of various applications have led to significant advancements in new NTE systems, encompassing a wide range of chemical substances and preparation methods [22]. Chemical synthesis methods provide a multitude of approaches to achieve desired NTE behaviors and associated properties in target compounds with specific structures. The chemical diversity is evident, with a broad regulatory scope and versatile introduction methods, and rich structure–function understanding (Scheme 2). One notable example of NTE behavior is found in the perovskite-type ferroelectric $PbTiO_3$ (PT), which was reported by Xing's group [23] in 2002 to exhibit NTE from room temperature to its Curie temperature (T_C = 763 K). The studies on the crystal structure and phase transitions of PT date back to the early 1950s [24]; however, the NTE characteristics of PT did not receive significant attention until the systematic investigation by Xing's group. Since then, NTE in PT-based ferroelectrics has garnered considerable research interest.

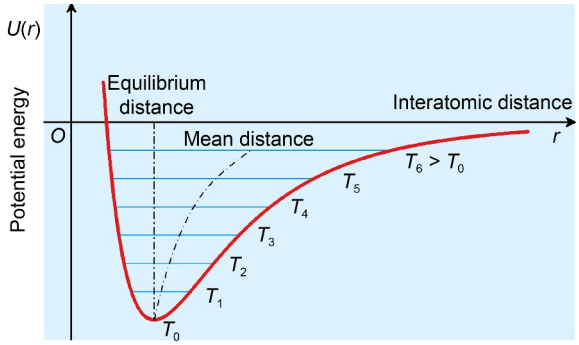

SCHEME 1 | Interatomic bonding potential, illustrating variation of potential energy with interatomic distance for a pair of bonded atoms. Vibrational energy levels are quantized, and with increasing temperature, the occupation of higher levels leads to a slight increase in the mean interatomic distance relative to the minimum-energy equilibrium distance, as shown.

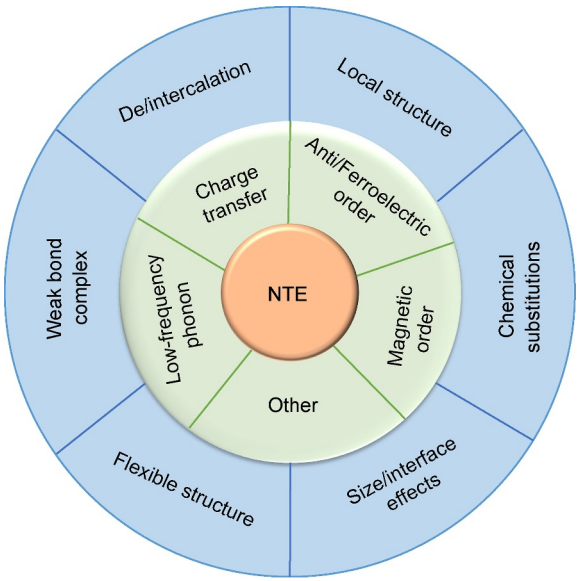

SCHEME 2 | Chemical diversity in tailoring of NTE. Reproduced with permission from Ref. [22]. Copyright 2022, American Chemical Society.

In 2004, simple perovskite MnF_3 was reported to show atypical NTE below its Néel temperature, characterized by an A-type magnetic spin ordering [25]. Later, in 2010, Wilkinson et al. reported an extraordinary NTE phenomenon in cubic ScF_3 [26], which exhibited a CTE larger than that of ZrW_2O_8. The identification of giant NTE in antiferromagnetic antiperovskite $Mn_3Zn_{1-x}Ge_xN$ further propelled research in the field of NTE [27], uncovering various NTE materials through mechanisms such as phonon-related transverse cooperative vibration [1, 28–47], magnetic transition [48–61], charge-transfer [62–66], metal-insulator phase transitions in Ruthenates [67–69], and spontaneous volume ferroelectrostriction in ferroelectrics [70–81]. In recent years, the concept of phase-transition-type NTE has dominated the field, with significant findings such as the large NTE observed in charge-transfer-induced phase transitions of double perovskite $LaCu_3Fe_4O_{12}$ in 2009 [62], and colossal NTE in $BiNiO_3$ driven by intermetallic charge transfer, as reported by Azuma's group [63]. Since then, phase-transition-type NTE materials have been developed and widely studied [82–86]. These NTE materials typically operate within a temperature range of several tens to 100 K near the phase transition. However, they can demonstrate negative CTE values significantly exceeding those of traditional NTE materials, enhancing their appeal for various applications.

1.3 | NTE in $PbTiO_3$-Type Perovskites

Despite the wide range of substances exhibiting NTE, the number of materials that display this behavior remains relatively limited. Continued research is essential to discover and develop new NTE materials to expand the existing family of such compounds. $PbTiO_3$, a perovskite-type (ABO_3) ferroelectric, stands out for its notable NTE characteristics, particularly from room temperature up to its Curie temperature (T_C = 763 K), with a large average volumetric CTE of -1.99×10^{-5} K^{-1} [87]. The structural flexibility of $PbTiO_3$ enables effective CTE control via chemical substitutions at the A-site (Pb) and/or B-site (Ti) atoms [88–97], as well as the less frequently studied substitutions at the oxygen site [98].

For instance, common A-site substitutions for Pb, such as $Pb_{1-x}Ba_xTiO_3$ [88], $Pb_{1-x}Sr_xTiO_3$ [89], $Pb_{1-x}Cd_xTiO_3$ [90], $Pb_{1-x}(La_{1/2}K_{1/1})_xTiO_3$ [99], and $Pb_{1-x}Bi_xTiO_3$ [91], usually lead to a decrease in NTE when compared with pristine $PbTiO_3$. Similar phenomena have also been observed in B-site substitutions of $PbTi_{1-x}Fe_xO_3$ [92], and A/B-site co-substitutions such as (1-x)$PbTiO_3$-xBi$(Ni_{1/2}Ti_{1/2})O_3$ [94] and (1-x)$PbTiO_3$-xBi$(Mg_{1/2}Ti_{1/2})O_3$ [100]. Enhanced NTE can be observed in compositions such as $(Pb_{1-x}Cd_x)TiO_3$ [90], (1-x)$PbTiO_3$-$x$$BiFeO_3$ [101], (1-x)$PbTiO_3$-$x$$PbVO_3$ [93], (1-x)$PbTiO_3$-$x$$BiLuO_3$ [102], and (1-x)$PbTiO_3$-$x$$BiCoO_3$ [95]. Notably, favorable zero thermal expansion can also be achieved in PT-based compounds through appropriate chemical substitutions [100, 103, 104]. Recent studies have emphasized the role of mixed-anion control in enhancing NTE in the oxysulfide of $PbTiO_3$ [98]. A comprehensive review by Chen et al. delves into the chemical modifications affecting the NTE properties of $PbTiO_3$ [5]. It is believed that the NTE behavior in $PbTiO_3$-based compounds primarily depends on the contraction of the polar c-axis in the tetragonal phase. An increase in the tetragonality (c/a) is expected to lead to a more pronounced NTE effect. Indeed, an intrinsic giant volume contraction of $V = -3.7\%$ was reported in $0.7PbTiO_3$-$0.3PbVO_3$ (c/a = 1.11), achieved by enhancing the tetragonality of $PbTiO_3$ [93].

$PbVO_3$, which exhibits the same tetragonal perovskite structure as $PbTiO_3$ (space group $P4mm$), demonstrates more pronounced lattice distortion (c/a = 1.23) and polarization (P_S = 101 μC cm^{-2}) based on point charge model calculations [105–108]. The tetragonal structure is stabilized by the stereochemical activity of Pb^{2+} and the strong Pb–O covalency, similar to that observed in $PbTiO_3$. The V^{4+} ion, characterized by a $3d^1$ electronic configuration, favors pyramidal coordination, which enhances the t_{2g} degeneracy and results in a stabilized $3d_{xy}$ orbital while destabilizing the degenerate $3d_{yz}$ and $3d_{zx}$ orbitals [109]. The presence of a single d electron in the $3d_{xy}$ orbital leads to an enhancement of the pyramidal distortion due to the Jahn–Teller effect.

Interestingly, $PbVO_3$ demonstrates a significant pressure-induced volume shrinkage of approximately 10.6% during phase transitions [106, 110], positioning it as a promising candidate for large NTE materials. However, the substantial structural distortion associated with $PbVO_3$ leads to a low decomposition temperature (T_d) of approximately 700 K [106], complicating the observation of a temperature-induced tetragonal-to-cubic phase transition that would result in NTE. To address this, researchers have employed a unique high-pressure and high-temperature synthesis method (Scheme 3) to stabilize $PbVO_3$ at elevated temperatures, thereby enhancing its thermal stability and enabling the observation of NTE in $PbVO_3$ and its derivatives.

This concise review summarizes the latest progress in exploring NTE in $PbVO_3$-based compounds spanning recent years. The exploration of NTE materials continues to be a vibrant field of research, with ongoing investigations seeking to uncover new compounds and mechanisms that can contribute to the development of materials with tailored thermal expansion properties. The implications of these discoveries extend across various

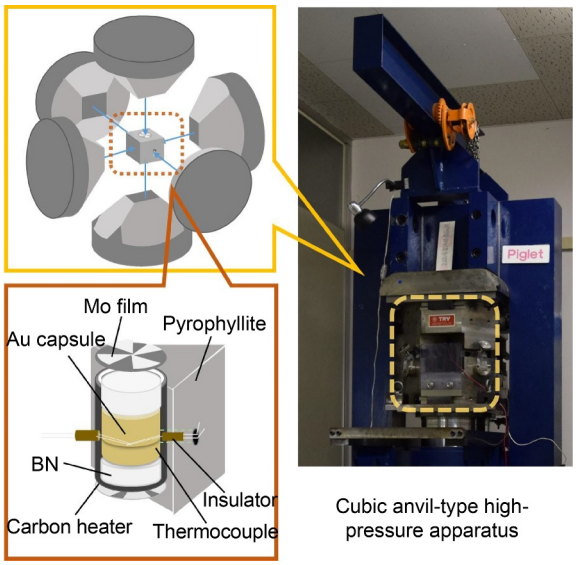

SCHEME 3 | High-pressure synthesis apparatus.

applications, from structural engineering to advanced electronic devices, underscoring the significance of NTE materials in modern technology.

2 | NTE in $PbVO_3$-Based Compounds

2.1 | Achieving NTE in $PbVO_3$ by A-Site Modification

$PbVO_3$ exhibits a colossal volume contraction accompanying the ferroelectric-to-paraelectric phase transition at a high pressure (~3 GPa). The magnitude of the intrinsic volume contraction reaches 10.6% [106, 110]. The substantial volume change suggests a major reconfiguration of the crystal structure upon heating during the phase transition. As a result, NTE is observed during the transition from the ferroelectric to the paraelectric phase. However, $PbVO_3$ decomposes at temperatures far below the T_C, which poses a significant obstacle as it prevents the observation of the ferroelectric-to-paraelectric phase transition that could potentially be accompanied by NTE. In the context of materials research, this limitation restricts the exploration of $PbVO_3$ as a potential new NTE material that relies on its phase transition. To overcome this challenge, researchers turned to electron doping of $PbVO_3$ in order to stabilize its metastable crystal structure. It was observed that electron doping of $PbVO_3$, achieved by substitution of Bi^{3+} for A-site Pb^{2+} by high-pressure synthesis (6 GPa, 1473 K), can effectively suppress the significant tetragonal distortion and destabilize the tetragonal phase of $PbVO_3$ [111]. The $Pb_{1-x}Bi_xVO_3$ (x = 0, 0.1, 0.2, and 0.3) compounds show a typical perovskite structure with a decrease tendency in c/a as a function of Bi^{3+} content (Figure 1A,B). As a result, the $Pb_{0.8}Bi_{0.2}VO_3$ compound undergoes a temperature-induced structural transition from tetragonal ferroelectric to cubic paraelectric (Figure 1C,D), resulting in an approximate 8% volume contraction (Figure 2A,B). Further increasing the Bi^{3+} content can still maintain a volume shrinkage value as high as 6.2% (Figure 2C,D). Such volume contractions of two coexisting phases of identical composition yet different structure (a homo-composite) have also been observed in $BiNiO_3$-based materials and can practically be considered as NTE. It should be mentioned that the changes in lattice parameters exhibit significant anisotropy.

To achieve NTE around room temperature, the substitution of lanthanum for lead in the $Pb_{0.8}Bi_{0.2}VO_3$ compound was investigated [111]. Notably, substitution of a minor amount of La^{3+} for Pb^{2+} diminishes the stereochemical activity of A-site cations and further lowers the tetragonal-to-cubic phase transition temperature. In particular, the $Pb_{0.76}La_{0.04}Bi_{0.20}VO_3$ compound demonstrates a significant NTE effect of approximately 6.7% in the vicinity of room temperature (230–410 K), as depicted in Figure 2E. Interestingly, the macroscopic volume change, $\Delta V/V \approx 3\Delta L/L$, estimated from the dilatometric measurement on a sintered body was approximately 8.5%, which is higher than the microscopic value derived from lattice parameter changes (Figure 2F). The linear CTE reached $\alpha_L = -590$ ppm K^{-1} within the temperature range of 280–310 K. A comparable effect was noted in the case of $Ca_2RuO_{3.72}$, where a sintered body with anisotropic crystallographic volume expansion demonstrated an enhanced dilatometric NTE.

The electron-doped $PbVO_3$ undergoes a first-order phase transition, characterized by the coexistence of low-temperature (LT) and high-temperature (HT) phases with significant volume disparity. During the heat treatment process, the relative proportions of the LT and HT phases shift, resulting in a progressive reduction of the average unit cell volume as the transition progresses. Typically, this material can be called a 2-phase type NTE material, which was also observed in other perovskite NTE materials [63]. The simultaneous presence of the LT and HT phases with identical composition, where their phase fractions alter as a function of temperature, contradicts Gibbs' phase law. This results from the disrupted pressure difference at the phase boundary between the LT and HT phases. This kind of coexistence of LT and HT phases at operating temperature is often observed in phase-transition-type NTE materials such as $BiNiO_3$ and its derivatives [63]. However, the atomic-scale structure at the phase boundary and domain structure remain unclear. The domain structure of the LT and HT phases may influence NTE, as variations in ferroelectric and piezoelectric properties are significantly dependent on the domain configuration. A recent study investigated the impact of electron doping and the reduction of $6s^2$ lone pair activity in $PbVO_3$ through the substitution of Bi^{3+}, Sr^{2+}, and La^{3+} for Pb^{2+} by high-pressure synthesis (8 GPa, 1373–1473 K) [86]. Sr^{2+} substitution stabilizes the cubic phase while maintaining the c/a ratio of the tetragonal phase, as shown in Figure 3A,B, where blue, red, and green denote tetragonal, cubic, and their coexistence, respectively. Recent studies have shown that the designed compounds $Pb_{0.8}Bi_{0.1}Sr_{0.1}VO_3$ and $Pb_{0.775}Bi_{0.125}Sr_{0.1}VO_3$ exhibit significant volume shrinkages of 9.3% and 8.4%, respectively, as depicted in Figure 3C,D, where blue, red, and black denote tetragonal phase, cubic phase, and weighted average volume, respectively. Note that a coexistence of tetragonal and cubic phases can be observed in a certain temperature range, as shown in Figure 3E, F, where blue and red denote tetragonal and cubic phases. Here, the observed NTE represents the largest shrinkages reported till date, highlighting the potential of these compounds in applications where precise control of thermal expansion is crucial.

The atomic arrangement at the boundary between tetragonal and cubic phases was examined using high-angle annular dark-field scanning transmission electron microscopy (HAADF-STEM), and Bragg coherent X-ray diffraction imaging (Bragg-CDI) was used to analyze the spatial distribution of domains. The current Bragg coherent diffraction imaging (Bragg-CDI) investigation is centered on the cubic 200 (200_c) Bragg reflection. Figure 4A presents the experimentally observed three-dimensional Bragg diffraction pattern for the 200_c reflection. The distinctive spotty pattern, characteristic of coherent diffraction, is referred to as a speckle pattern. The presence of a streaky tail extending from the Bragg position, perpendicular to the scattering vector $\boldsymbol{Q}_{200}$, suggests the presence of an interface or surface with a normal vector orthogonal to $\boldsymbol{Q}_{200}$. Figure 4B illustrates a cross-sectional fast Fourier transform (FFT) image derived from Figure 4A. As the FFT image represents the autocorrelation function of the particle image, the longitudinal stripes observed indicate that multiple interfaces are approximately parallel to one another, as schematically depicted in Figure 4C. Figure 4D displays the reconstructed three-dimensional image of the particle, obtained through a phase retrieval calculation utilizing the data from Figure 4A. The isodensity surfaces depicted within the structure

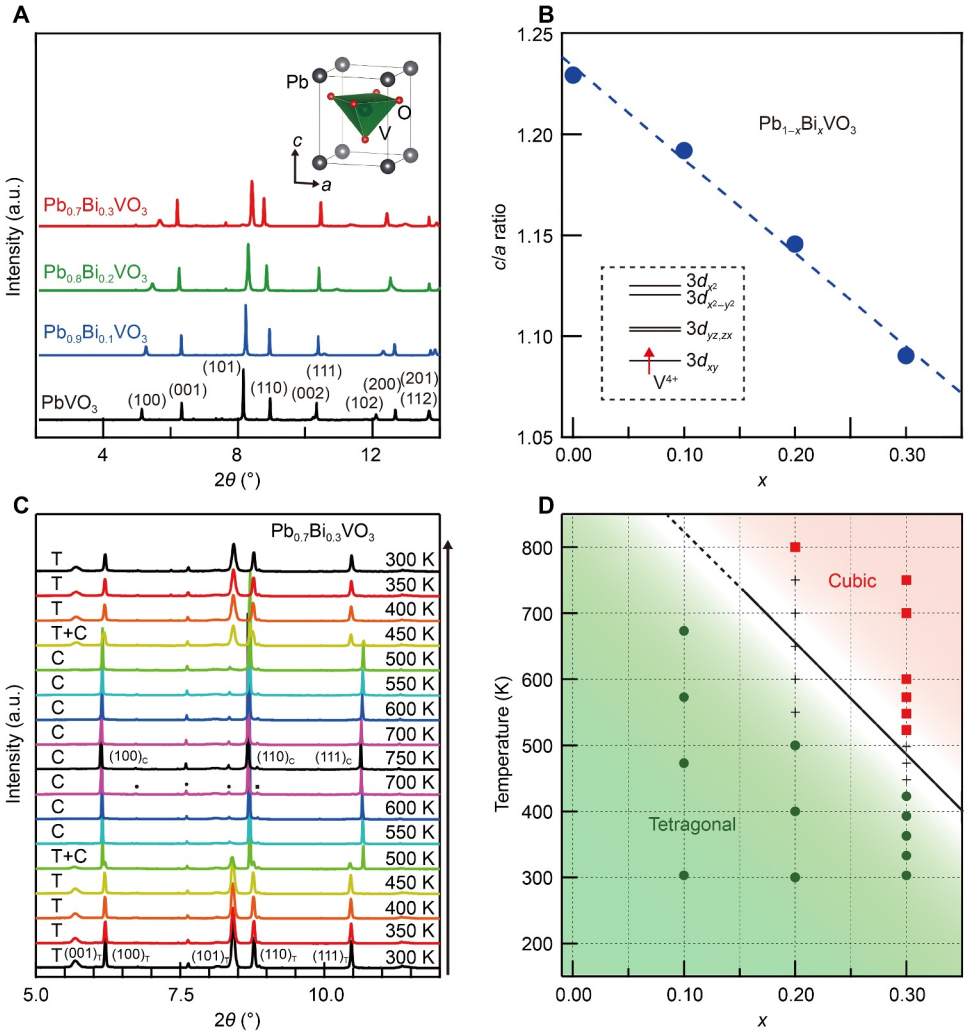

FIGURE 1 | (A) Synchrotron X-ray diffraction (SXRD) patterns of the $Pb_{1-x}Bi_xVO_3$ (x = 0, 0.1, 0.2, and 0.3) compounds; (B) composition dependence of c/a ratio of $Pb_{1-x}Bi_xVO_3$ (x = 0, 0.1, 0.2, and 0.3), and (inset) representation of energy levels of 3d orbitals in VO_5 pyramid; (C) temperature variation of SXRD data of the $Pb_{0.7}Bi_{0.3}VO_3$ compound; (D) composition–temperature phase diagram of $Pb_{1-x}Bi_xVO_3$. Reproduced with permission from Ref. [111]. Copyright 2018, Wiley VCH.

highlight regions of elevated 200_c reflection density. The cross-sectional views of the Bragg-CDI presented in Figure 4E,F are oriented parallel to the 011-connection interface and orthogonal to the $\boldsymbol{Q}_{200}$ direction, as depicted in Figure 4C. The methodology for determining these orientations is detailed in the Supporting information of Ref. [86]. The 200_c reflection density within the horizontal plane, as illustrated in Figure 4D, is further represented in Figure 4E. To achieve a seamless transition between the cubic and "tetragonal" (which is more accurately described as pseudo-orthorhombic or of lower symmetry) regions, the {110}-connection is posited as the most plausible configuration, based on symmetry considerations and the minimization of elastic energy. In the $Pb_{0.9}Sr_{0.1}VO_3$ compound, temperature changes did not alter the fractions of tetragonal and cubic phases. However, slight electron doping via Bi^{3+} substitution enhanced the NTE effect, maintaining a volume difference of approximately 11% [86]. Note that the temperature hysteresis in the $Pb_{0.775}Bi_{0.125}Sr_{0.1}VO_3$ compound was significantly suppressed after several temperature cycles, which could be attributed to the change of the domain structure.

NTE in metastable $PbVO_3$ can be realized by electron doping and reducing the $6s^2$ lone pairs of the A-site Pb cation. Although the former can effectively reduce the c/a ratio of $PbVO_3$, the latter can promote a transition from tetragonal to cubic phase. Accordingly, a temperature-induced transition from tetragonal ferroelectric to cubic paraelectric structure occurs, resulting in significant volume contraction.

2.2 | Achieving NTE in $PbVO_3$ by B-Site Modification

Substituting Bi^{3+} and La^{3+} for A-site Pb^{2+} in $PbVO_3$ introduces electron doping, which effectively reduces tetragonal distortion and facilitates the tetragonal-to-cubic phase transition upon heating [111]. This discovery is crucial as it introduces new possibilities for altering the structural and electronic properties of materials via doping. Replacing the B-site V^{4+} in $PbVO_3$ with other tetravalent transition-metal ions is expected to

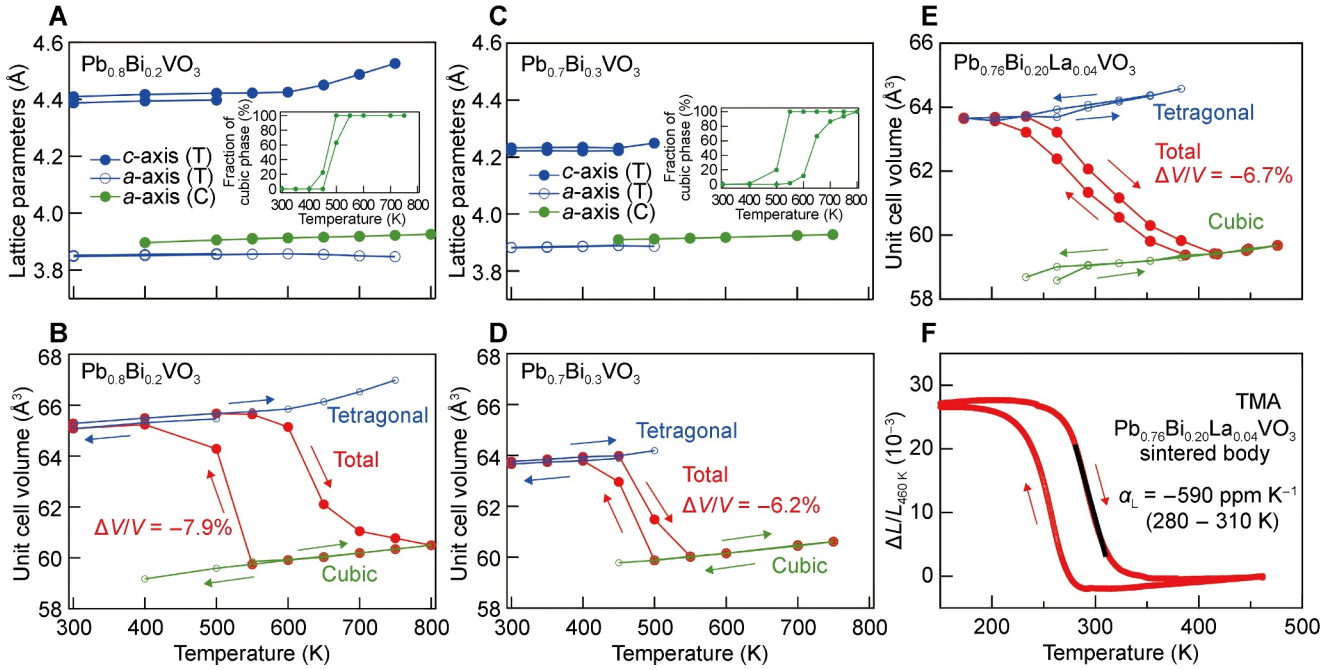

FIGURE 2 | (A) Temperature dependence of lattice parameters in $Pb_{0.8}Bi_{0.2}VO_3$, where (inset) evolution of cubic phase fraction; (B) temperature dependence of unit cell volume in $Pb_{0.8}Bi_{0.2}VO_3$; (C) temperature dependence of lattice parameters in $Pb_{0.7}Bi_{0.3}VO_3$, where (inset) evolution of cubic phase fraction; (D) temperature dependence of unit cell volume in $Pb_{0.7}Bi_{0.3}VO_3$; (E) temperature dependence of cell volume in $Pb_{0.76}La_{0.04}Bi_{0.20}VO_3$; (F) temperature dependence of linear thermal expansion $\Delta L/L$, where dilatometric volume change can be estimated using relation $(3\Delta L/L \approx \Delta V/V)$. Reproduced with permission from Ref. [111]. Copyright 2018, Wiley VCH.

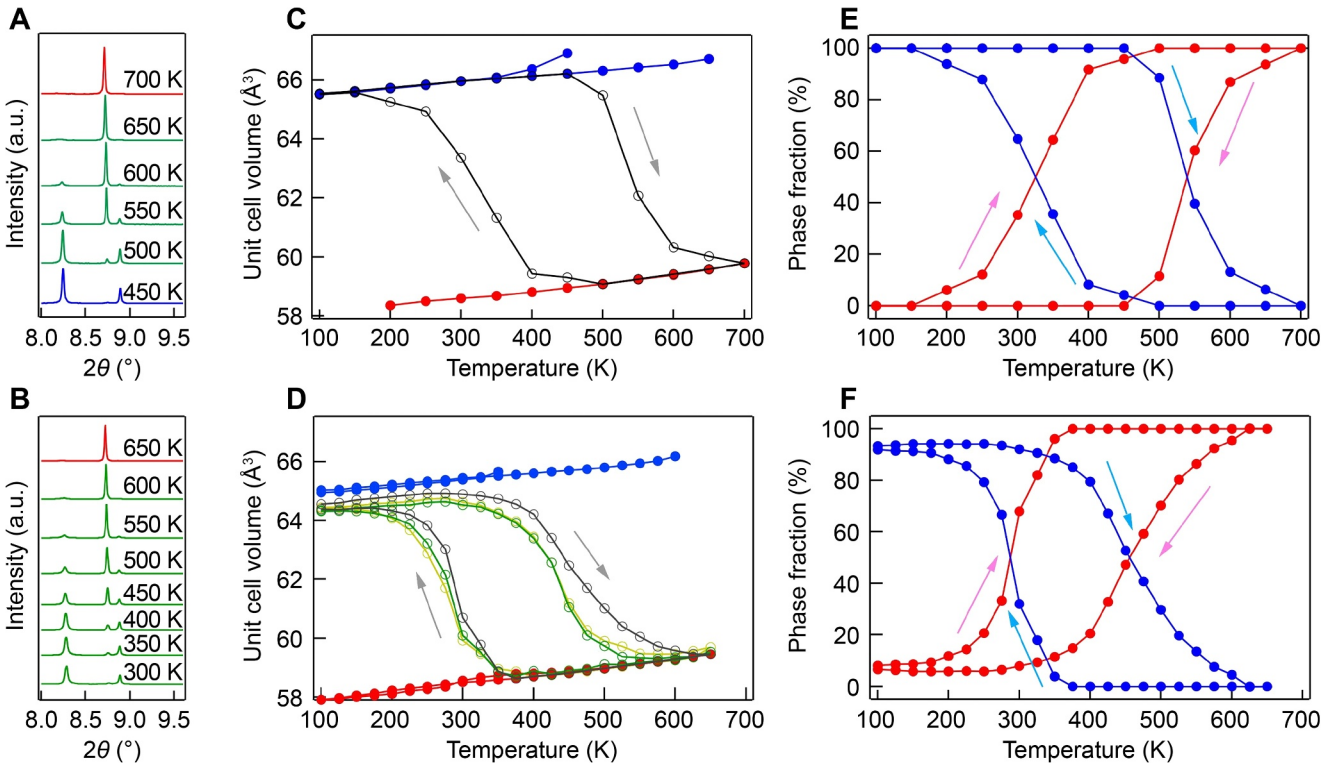

FIGURE 3 | Temperature dependence of SXRD patterns of (A) $Pb_{0.8}Bi_{0.1}Sr_{0.1}VO_3$ and (B) $Pb_{0.775}Bi_{0.125}Sr_{0.1}VO_3$ around 110_T, 101_T, and 110_C. Temperature dependence of unit cell volume of (C) $Pb_{0.8}Bi_{0.1}Sr_{0.1}VO_3$ and (D) $Pb_{0.775}Bi_{0.125}Sr_{0.1}VO_3$, and heating/cooling cycles were repeated 10 times for $Pb_{0.775}Bi_{0.125}Sr_{0.1}VO_3$, but only data for first, fifth (green), and tenth (yellow) cycles were plotted; temperature dependence of phase fraction of tetragonal and cubic phases in (E) $Pb_{0.8}Bi_{0.1}Sr_{0.1}VO_3$ and (F) $Pb_{0.775}Bi_{0.125}Sr_{0.1}VO_3$. Reproduced with permission from Ref. [86]. Copyright 2023, American Chemical Society.

disrupt d_{xy} orbital ordering, thereby inducing the tetragonal-to-cubic structural change accompanied by a volume shrinkage. Indeed, the high-pressure synthesized (6 GPa, 1373 K) $Pb(V_{0.1}Ti_{0.9})O_3$ compound exhibits a significant nonlinear NTE across a broad temperature range (Figure 5A), with an average volumetric CTE of $\overline{\alpha}_V = -3.76 \times 10^{-5}$ K^{-1} between 300 and 823 K, was observed by the partial substitution of Ti^{4+} for V^{4+} [93]. Notably, a significant intrinsic volume contraction of up to 3.6% was observed in $Pb(V_{0.7}Ti_{0.3})O_3$ during its transition from the ferroelectric to paraelectric phase (Figure 5C). The observed volume contraction closely corresponds to the phenomenon of spontaneous volume ferroelectrostriction (SVFS), as illustrated in Figure 5A–C, which is a key factor in the NTE of ferroelectric materials. Additionally, the suppression of tetragonal distortion and the decrease in spontaneous polarization were also observed in the $PbV_{1-x}Cr_xO_3$ system by high-pressure synthesis (8 GPa, 1273–1473 K) [112], as confirmed by structural refinements based on synchrotron X-ray powder diffraction (SXRD). As expected, the suppressed tetragonal distortion enabled the tetragonal-to-cubic phase transition (Figure 6A–C), which is accompanied by NTE, as shown in Figure 6. It is worth noting that a temperature-induced semiconductor-to-metal transition was also observed in the $PbV_{1-x}Cr_xO_3$ system.

The NTE properties of $PbV_{1-x}Cr_xO_3$ were compared with those of the aforementioned $Pb(V_{0.9}Ti_{0.1})O_3$. $Pb(V_{0.9}Ti_{0.1})O_3$ exhibits NTE and achieves a maximum volume contraction of 3.6% at a low V concentration of $x = 0.30$ ($c/a = 1.10$) [112]. Samples with $x > 0.40$ decompose far below the tetragonal-to-cubic transition temperature, similar to those of pristine $PbVO_3$. Experimental and theoretical studies indicate the pivotal role of ferroelectric properties in the NTE behavior of lead-based ferroelectrics.

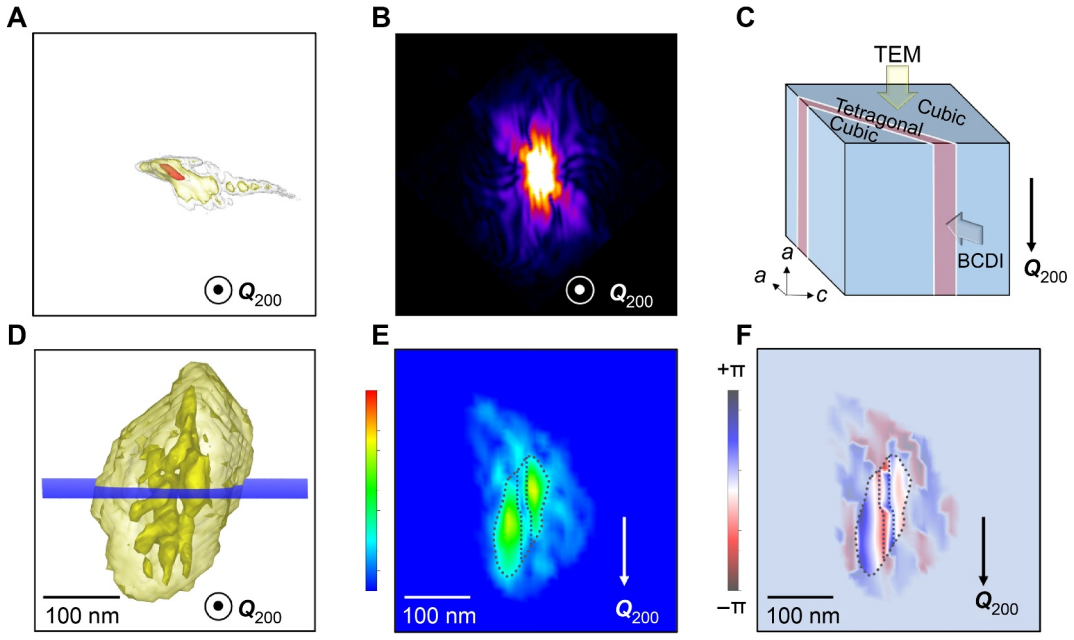

FIGURE 4 | Bragg-CDI of $Pb_{0.82}Sr_{0.18}VO_3$ sample: (A) single recorded diffraction pattern; (B) cross-sectional FFT image of (A); (C) schematic illustration of cubic-tetragonal interfaces; (D) reconstructed three-dimensional image of particle; (E) cubic 200 reflection density map in horizontal plane in (C); (F) phase image of same plane in (E). Reproduced with permission from Ref. [86]. Copyright 2023, American Chemical Society.

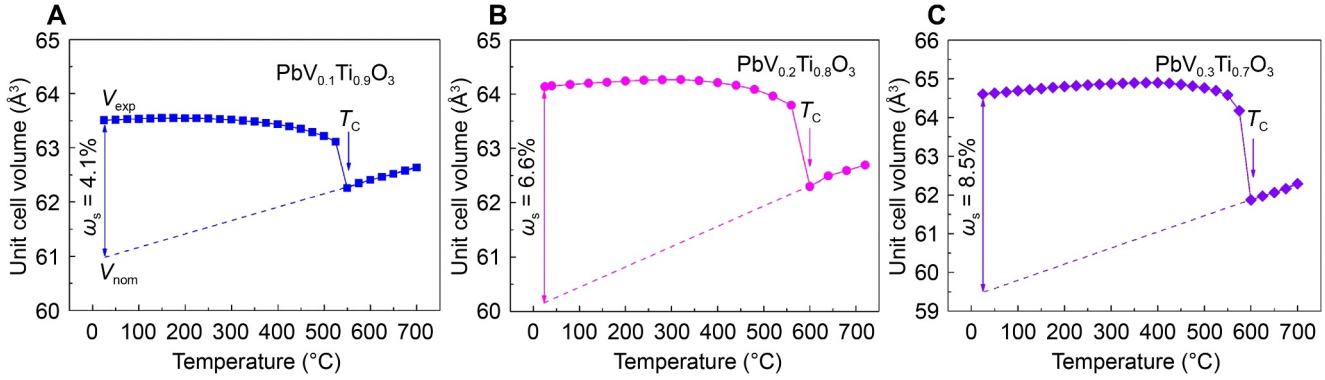

FIGURE 5 | Temperature dependence of unit cell volume for (A) $PbV_{0.1}Ti_{0.9}O_3$, (B) $PbV_{0.2}Ti_{0.8}O_3$, and (C) $PbV_{0.3}Ti_{0.7}O_3$, respectively, where SVFS and volume change are indicated. Reproduced with permission from Ref. [93]. Copyright 2017, American Chemical Society.

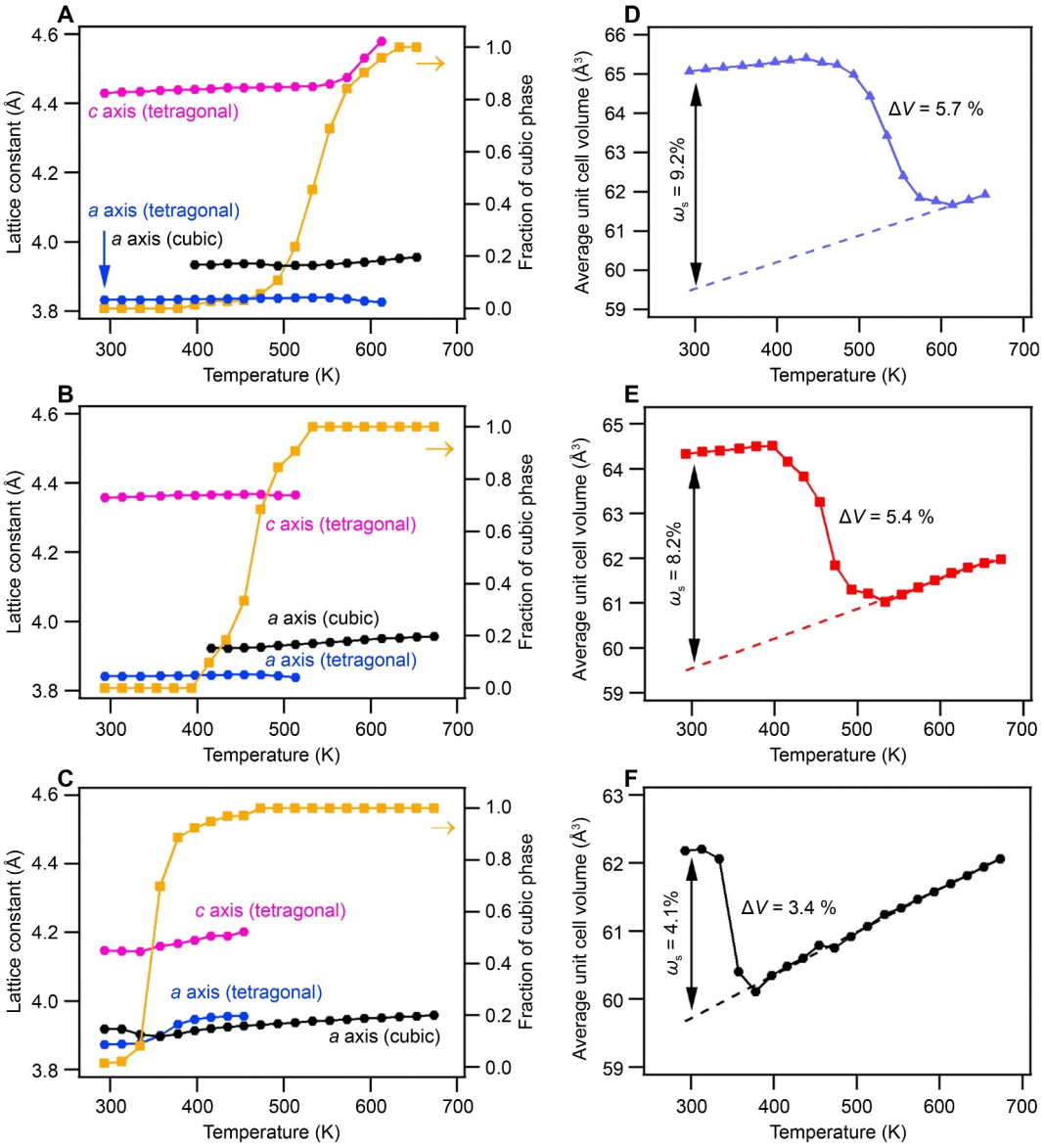

FIGURE 6 | Temperature dependence of refined lattice parameters and fraction of cubic phase for (A) $PbV_{0.85}Cr_{0.15}O_3$, (B) $PbV_{0.80}Cr_{0.20}O_3$, and (C) $PbV_{0.75}Cr_{0.25}O_3$ measured on heating; (D–F) corresponding unit cell volumes as a function of temperature, where volume shrinkage ΔV between NTE and SVFS, ω_S is provided in each graph. Reproduced with permission from Ref. [112]. Copyright 2019, American Chemical Society.

Recently, a novel concept, spontaneous volume ferroelectrostriction (SVFS), has been introduced to quantitatively assess the role of ferroelectricity in NTE materials. The Debye–Grüneisen equation, which incorporates the Grüneisen parameter, is commonly used to estimate the thermal expansion of solids by considering phonon contributions. By excluding the effects of anharmonic phonon vibrations, the impact of physical properties such as ferroelectric and magnetic orderings on NTE can be directly and quantitatively assessed. Thermal expansion in $PbV_{1-x}Cr_xO_3$ is minimal at low temperatures, approaching zero at 0 K, due to contributions from anharmonic lattice phonon vibrations and ferroelectric order affecting the unit cell volume. As temperature decreases, the impact of anharmonic lattice phonon vibrations diminishes. The nominal unit cell volume (V_{nm}), extrapolated from data in the paraelectric region, is expected to contract as described by the Debye–Grüneisen equation. The specifics of SVFS can be assessed using the Equation (2) [70],

$$\omega_S = \frac{V_{exp} - V_{nm}}{V_{nm}} \times 100\%, \quad (2)$$

where V_{exp} denotes the experimental unit cell volume, ω_S indicates the spontaneous volume ferroelectrostriction. A high ω_S value signifies a strong ferroelectrovolume effect and enhanced NTE, whereas a low ω_S value suggests weak NTE. The current ω_S of $PbV_{0.85}Cr_{0.15}O_3$ might be overestimated due to the cubic phase being limited to a 100 K temperature range, resulting in some ambiguity in estimating V_{nm}. As shown in Figure 6, the values of ω_S are 9.2%, 8.2%, and 4.1% for the $PbV_{0.85}Cr_{0.15}O_3$ (Figure 6D), $PbV_{0.80}Cr_{0.20}O_3$ (Figure 6E), and $PbV_{0.75}Cr_{0.25}O_3$ (Figure 6F), respectively. This means that Cr substitution diminishes the

ferroelectrovolume effect, aligning with the observed reduction in the c/a ratio. In comparison, the current ω_S of $PbV_{0.85}Cr_{0.15}O_3$ significantly exceeds many $PbTiO_3$-based ferroelectric NTE materials, including pristine $PbTiO_3$ (3.1%), $0.5PbTiO_3$-$0.5BiFeO_3$ (5%), and the recently reported $0.5PbTiO_3$-$0.5BiCoO_3$ (7.2%). It even surpasses the value of $PbV_{0.30}Ti_{0.70}O_3$ (8.5%), demonstrating a more pronounced ferroelectrovolume effect. This aligns with the larger volume shrinkage of $PbV_{0.85}Cr_{0.15}O_3$ observed during the ferroelectric-to-paraelectric phase transition. Figure 7 illustrates the relationship between ω_S and Pb displacement δz_{Pb}^2 of $PbV_{1-x}Cr_xO_3$ and $PbV_{1-x}Ti_xO_3$. A strong linear correlation between ω_S and δz_{Pb}^2 is evident and can be expressed as follows:

$$\omega_S \sim \alpha \delta z_{Pb}^2, \quad (3)$$

where α represents the coupling coefficient between ω_S and δz_{Pb}. The relationship between ω_S and δz_{Pb} is based on a large number of experimental results [70]. Analogous to Landau theory, a significant correlation is observed in Pb-based ferroelectrics. The SVFS effect observed in ferroelectrics is analogous to the spontaneous volume magnetostriction effect found in magnetic materials. $PbV_{0.85}Cr_{0.15}O_3$ exhibits a larger δz_{Pb} than that of $PbV_{0.30}Ti_{0.70}O_3$, resulting in an increased ω_S and a stronger ferroelectrovolume effect, and therefore a more pronounced NTE effect.

NTE in metastable $PbVO_3$ has been realized through B-site chemical modifications, specifically by introducing Ti/Cr dopants. The tetragonal distortion of $PbVO_3$ can be effectively suppressed through the substitutions. Consequently, compounds with reduced tetragonal distortion undergo a temperature-induced transition from a tetragonal to a cubic structure, accompanied by NTE. This discovery is of great significance, as it provides a strategy for manipulating the thermal expansion properties of materials, which is crucial for various applications, including high-temperature ceramics, aerospace components, and electronic devices. The mechanism behind the NTE behavior in these materials is closely related to the electronic and structural changes that occur during the phase transition. In the case of $PbVO_3$, the substitution of Ti or Cr for V leads to a change in the electronic configuration, which in turn affects the crystal field and the orbital ordering. This disruption of the d_{xy} orbital ordering destabilizes the tetragonal phase, allowing for the transition to a cubic phase at higher temperatures. The cubic phase has a lower volume than the tetragonal phase, thus resulting in a net volume contraction and NTE.

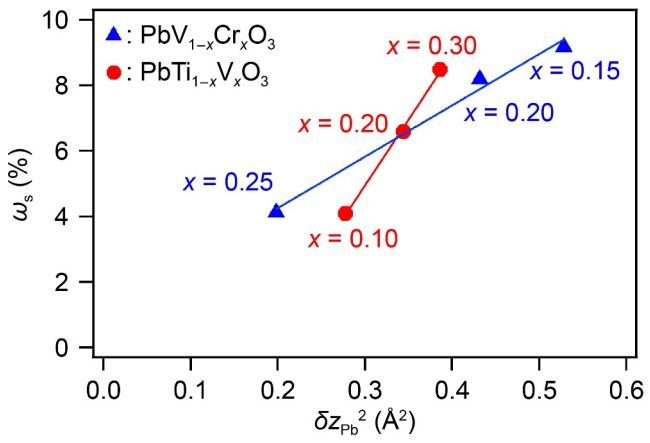

FIGURE 7 | Plot of ω_S versus Pb displacement δz_{Pb}^2 for $PbVO_3$-based $PbV_{1-x}Cr_xO_3$ and $PbTiO_3$-based $PbV_{1-x}Ti_xO_3$. Reproduced with permission from Ref. [112]. Copyright 2019, American Chemical Society.

2.3 | Achieving NTE in $PbVO_3$ by Anion Oxygen-Site Modification

Substituting Bi^{3+} for Pb^{2+} and Ti^{4+} for V^{4+} in $PbVO_3$ decreases tetragonal distortion, facilitating a tetragonal-to-cubic phase transition upon heating and resulting in NTE [93]. Especially, $Pb(V_{1-x}Ti_x)O_3$ is a notable NTE material, as the $PbV_{0.1}Ti_{0.9}O_3$ compound exhibits a strong NTE over a wide temperature range [93]. Additionally, the NTE operation temperature of $Pb_{1-x}Bi_xVO_3$, which exhibits NTE near 600 K with a 7.9% volume reduction, can be shifted to room temperature by substitution of additional La^{3+}. The $Pb_{0.76}La_{0.04}Bi_{0.20}VO_3$ compound exhibits NTE with a dilatometric linear CTE $\alpha_L = -590$ ppm K^{-1} over the temperature range of 280–310 K. These imply that electron doping is efficient to realize NTE in $PbVO_3$.

Research studies on modifying the thermal expansion properties of perovskite-type ferroelectric materials have predominantly concentrated on cation substitutions at the A- and B-sites, with limited attention paid to substitutions at the anion O-site. The challenge in synthesizing mixed-anion perovskite compounds may account for this issue. However, the differences in the valences, electronegativities, and ionic radii of heteroanions are expected to affect the crystal and electronic structure of perovskite materials [113, 114], and therefore, modify the thermal expansion behavior. Recently, an exceptionally enhanced NTE with an average volumetric CTE of $\overline{\alpha}_V = -2.50 \times 10^{-5}$ K^{-1} was achieved over a wide temperature range (300–790 K) in the $PbTiO_{3-x}S_x$ compound through the substitution of S for O in $PbTiO_3$ [98], which is in contrast to that of pristine $PbTiO_3$ ($\overline{\alpha}_V = -1.99 \times 10^{-5}$ K^{-1}, RT ~ 763 K). The intensified NTE is attributed to the enhanced hybridization between Pb and O/S atoms by the substitution of S, which was evidenced by the first-principles calculations. Therefore, introducing mixed anions is a promising approach for managing thermal expansion in perovskite ferroelectrics.

Recently, the $PbVO_{3-x}F_x$ system, where O^{2-} was partially replaced by F^-, was designed and prepared by the high-pressure and high-temperature synthesis method (8 GPa, 1473 K) [115]. Mixed anions with varying valences can serve as electron or hole dopants for the cation. Replacing O^{2-} with F^- offers an alternative method for electron doping in V^{4+} within $PbVO_3$. XRD data indicate that increasing F^- content at the anion sites of $PbVO_3$ reduces tetragonal distortion, similar to observations in $Pb_{1-x}Bi_xVO_3$, and further substitution leads to the emergence of a cubic phase with a $Pm\bar{3}m$ space group (Figure 8). For the $PbVO_{2.79}F_{0.21}$ compound, a coexistence of tetragonal and cubic phase can be observed at room temperature. Upon further substitution, the tetragonal phase vanishes, resulting in a sole cubic phase in the $PbVO_{2.78}F_{0.22}$ compound. The Rietveld refinement results allow for the determination of the composition dependence of the c/a ratio, unit cell

volume, as well as spontaneous polarization (P_S) derived from the refined parameters. Notably, all parameters progressively decrease with the increase of F concentration. It is worth noting that the P_S of F-substituted samples is smaller than that of Bi-substituted samples, despite a less significant reduction in the c/a ratio. Figure 9 compares the ion displacements and their contributions to the spontaneous polarizations in $PbVO_3$, $PbVO_{2.80}F_{0.20}$, and $Pb_{0.80}Bi_{0.20}VO_3$. The significant decrease in P_S of F-substituted samples is attributed to the reduction in hybridization between Pb^{2+} and O^{2-}/F^{-}.

XRD experiments were conducted to investigate the temperature-dependent thermal expansion properties of F-substituted $PbVO_3$ samples. A temperature-induced tetragonal-to-cubic phase transition accompanied by NTE was observed in the $PbVO_{2.79}F_{0.21}$ compounds. Figure 10A shows the temperature dependence of the XRD patterns during both heating and cooling. The intensity ratio between the tetragonal and cubic phases varies with the heating and cooling processes, suggesting a first-order transition.

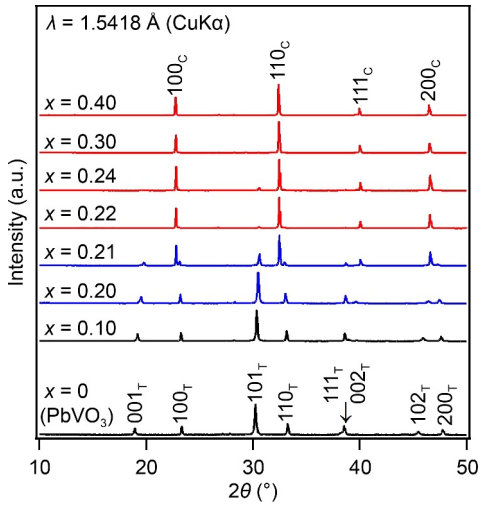

FIGURE 8 | XRD patterns of $PbVO_{3-x}F_x$ ($x = 0$, 0.10, 0.20, 0.21, 0.22, 0.24, 0.30, and 0.40) at room temperature, where data with tetragonal, cubic, and mixed phases are displayed in black, red, and blue, respectively. Reproduced with permission from Ref. [115]. Copyright 2019, IOP Publishing.

This indicates that the splitting between tetragonal (100) and (001) peaks remains largely unchanged. Figure 10B depicts the temperature-dependent lattice parameters, cubic phase fraction, and weighted average unit cell volume in the top and middle panels, respectively. Despite thermal expansion in the lattice constants of both tetragonal and cubic phases, the reduction (or increase) in the proportion of the larger tetragonal phase and the corresponding increase (or decrease) in the smaller cubic phase during heating (or cooling) results in a decrease (or increase) in the average volume. This phenomenon contributes to NTE over the temperature range of 233–473 K, with an average linear CTE α_L of approximately -50 ppm K^{-1}. The maximum $\alpha_{Lmax} = -129$ ppm K^{-1} is observed at 293 K. Despite a 10.8% volume difference between tetragonal and cubic phases, the average unit cell volume decreases by 4.0% between 233 and 473 K, which is significantly less than the 7.9% reduction observed in the $Pb_{0.80}Bi_{0.20}VO_3$ compounds. This is due to the incomplete phase transition, where the cubic phase persists at the lowest temperature and the tetragonal phase at the highest.

The dilatometric curve of the sintered $PbVO_{2.79}F_{0.21}$ sample is depicted at the bottom of Figure 10B. NTE was observed within the same temperature range as the temperature dependence of the average unit cell volume (see the middle of Figure 10B). It is noteworthy that an unexpectedly large magnitude of NTE ($\alpha_L = \sim -358$ ppm K^{-1}) was observed. A dilatometric length change of approximately 4.5% for $\Delta L/L$ was observed, corresponding to the total volume shrinkage of $\Delta V/V$ approximately 13.5% was observed, which is three times as large as that estimated from the temperature dependence of average unit cell volume. Furthermore, the observed NTE effect surpasses that of previously reported $Pb_{0.76}La_{0.04}Bi_{0.20}VO_3$ material, which exhibited an 8.5% volume shrinkage [111]. The enhanced NTE in the sintered pellet can be explained by the anisotropic crystallographic volume expansion model suggested for $Ca_2RuO_{3.72}$. The anisotropic thermal expansion of needle-shaped crystals amplifies the NTE effect, attributed to the decrease in voids within the sintered body. The tetragonal phase of $PbVO_{2.79}F_{0.21}$ exhibits a larger c/a ratio of 1.17 compared to that of $Pb_{0.76}La_{0.04}Bi_{0.20}VO_3$ (1.10). During the tetragonal-to-cubic phase transition, the c axis decreases by approximately 14%, whereas the a axis increases by about 2%. The significant anisotropic thermal expansion could be the cause of the increased dilatometric NTE.

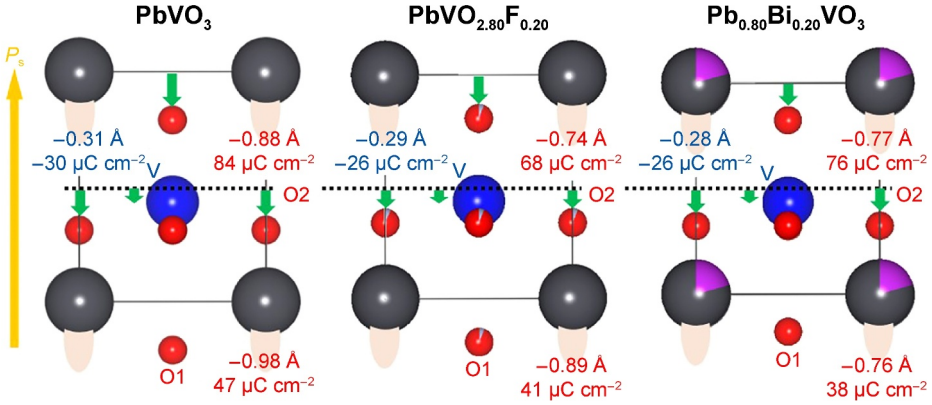

FIGURE 9 | Schematic drawings of tetragonal phases of $PbVO_3$, $PbVO_{2.80}F_{0.20}$, and $Pb_{0.80}Bi_{0.20}VO_3$, where ionic displacements from special positions and contributions to spontaneous polarization are indicated. Reproduced with permission from Ref. [115]. Copyright 2019, IOP Publishing.

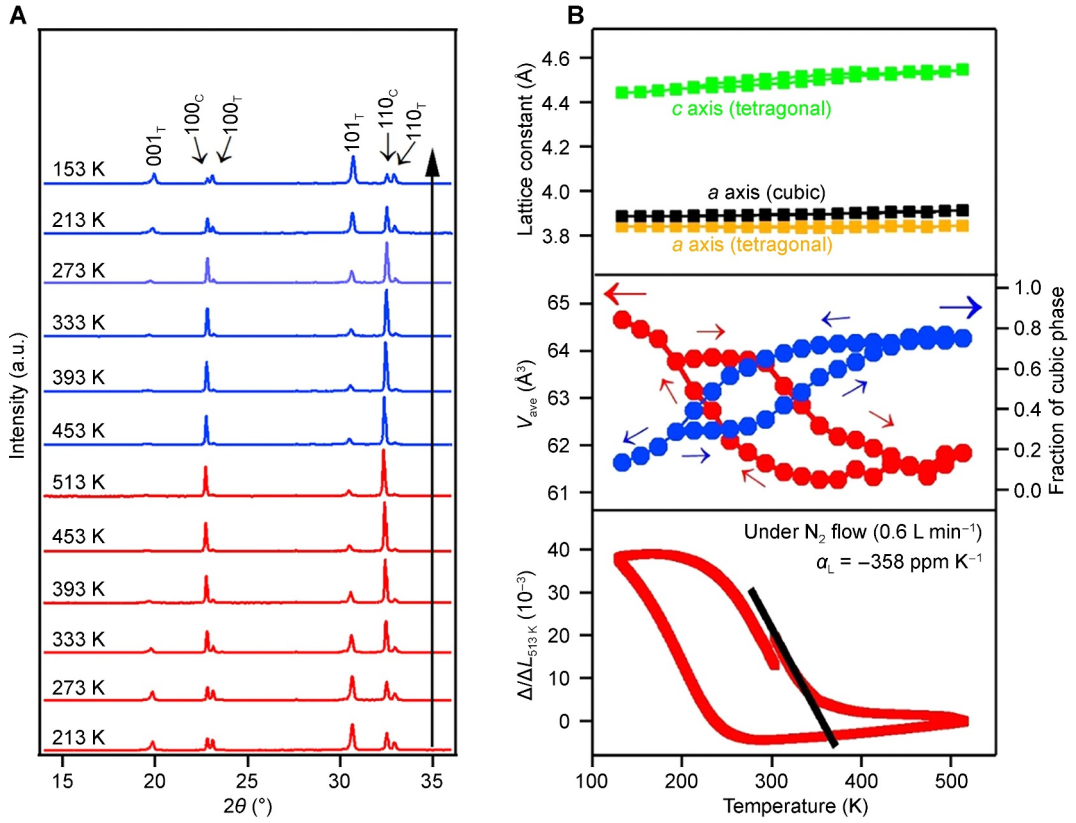

FIGURE 10 | (A) Temperature dependence of laboratory XRD data of $PbVO_{2.79}F_{0.21}$ on heating and cooling; (B) temperature dependence of lattice parameters (top), average unit cell volumes and refined phase fraction of cubic phase (middle), and the dilatometric curve for a sintered body of $PbVO_{2.79}F_{0.21}$ (bottom). Reproduced with permission from Ref. [115]. Copyright 2019, IOP Publishing.

The electron doping of $PbVO_3$ with V^{4+} ions and the substitution of F^- for O^{2-} destabilized its large tetragonal distortion, resulting in a tetragonal-to-cubic structural transition at $PbVO_{2.79}F_{0.21}$. This phenomenon is analogous to the doping-induced second-order ferroelectric transition observed in $BaTiO_3$, where the material undergoes a tetragonal-to-cubic phase transition at a critical doping concentration. A temperature-induced tetragonal-to-cubic phase transition accompanied by NTE was observed.

3 | Summary and Perspectives

In summary, significant advancements have been achieved in developing innovative NTE materials based on the $PbTiO_3$-type perovskite framework of metastable $PbVO_3$. The employment of cutting-edge sample preparation techniques and in situ synchrotron XRD analysis has played a crucial role in this pursuit. For example, the high-pressure and high-temperature synthesis approach enables the establishment of unique conditions conducive to stabilizing otherwise metastable phases, enabling the exploration of materials with distinct properties. This technique exposes materials to extreme pressures and temperatures, which can modify their crystal structures and electronic states, potentially leading to the emergence of NTE behavior. Simultaneously, synchrotron XRD experiments provide highly accurate and detailed information about the crystal structures of the materials. The intense and monochromatic X-ray beams from synchrotrons can penetrate the samples deeply, and the diffraction patterns obtained can be analyzed to determine the lattice parameters, phase compositions, and even the local atomic arrangements. The precision in understanding the structural implications of chemical substitutions is crucial for enhancing the thermal expansion properties of materials. These techniques have significantly advanced our understanding and contributed to the discovery of new NTE materials. The progress and prospects regarding the realization of NTE in $PbVO_3$ and its derivatives are elaborated as follows.

i. Electron-doping by substituting Bi^{3+} for the A-site Pb^{2+} in $PbVO_3$ has profound effects on its structure and properties. The substitution results in a decrease of the c/a ratio, serving as a critical indicator for tetragonal distortion within the crystal lattice. A lower c/a ratio implies a more symmetric structure, approaching the cubic phase. Moreover, it decreases the stability of the tetragonal phase. In the case of the $Pb_{0.80}Bi_{0.20}VO_3$ compound, when the temperature exceeds 650 K, it undergoes a temperature-induced transition to the cubic phase. This transition is accompanied by a significant volume change, with a $\Delta V/V$ of approximately −7.9%, demonstrating a remarkable NTE effect. The co-substitution of Pb^{2+} with Bi^{3+} and La^{3+} in $Pb_{0.76}La_{0.04}Bi_{0.20}VO_3$ is even more fascinating. This dual-substitution strategy effectively lowers the transition temperature to around room temperature. This is highly significant as it makes the NTE property more applicable in practical scenarios where ambient temperatures are common. With this co-substitution, the material exhibits an

NTE with a $\Delta V/V$ of about −6.7%, offering potential for applications in devices that require thermal stability at room temperature, such as microelectronics. Furthermore, the replacement of the A-site Pb^{2+} by Sr^{2+} in $PbVO_3$, as seen in $Pb_{0.9}Sr_{0.1}VO_3$, also disrupts the tetragonal distortion. The tetragonal c/a ratio of $Pb_{0.9}Sr_{0.1}VO_3$ is decreased to 1.19, and it shows a large volume difference of up to 11.1% from the cubic phase. Notably, a reversible temperature-induced phase transition occurs, accompanied by an extraordinary NTE of 9.3%. This reversibility is a valuable characteristic as it indicates that the material can repeatedly exhibit the NTE behavior with temperature cycling, which is highly desirable for applications where thermal cycling is involved, such as in some thermal management systems.

ii. Beyond A-site modifications, the large tetragonal distortion of $PbVO_3$ can be effectively reduced by replacing the B-site V with other 3d transition metals. When Ti is used to substitute B-site V in $PbVO_3$, the tetragonality of the crystal structure is notably decreased. This reduction in tetragonality leads to the achievement of NTE over a wide temperature range in the $PbV_{1-x}Ti_xO_3$ solid solutions. For the composition of $PbV_{0.3}Ti_{0.7}O_3$, an impressively large volume contraction of up to 3.7% has been observed. This large volume change is a clear indication of the strong NTE effect in this material. It is important to note that this is not an isolated case. The substitution of Cr for B-site V can also suppress the tetragonal distortion and spontaneous polarization. Compounds with suppressed tetragonal distortion often exhibit ferroelasticity, which means they can change their shape in response to an applied stress and return to their original shape when the stress is removed. Additionally, they undergo a temperature-induced tetragonal-to-cubic structural transition, which is accompanied by NTE. This shows that B-site modifications offer a versatile approach to tuning the NTE properties of $PbVO_3$-based materials, and different 3d transition metal substitutions can lead to a variety of interesting property combinations.

iii. Compared to the extensively studied A- and B-site modifications, the impact of substitutions at the anion O site on thermal expansion properties has received relatively little attention. However, recent research studies have shown that this is a promising area of exploration. Mixed anions with different valences can act as electron/hole doping agents for the cations. In the case of $PbVO_3$, substituting O^{2-} with F^- has been found to effectively suppress the stability of the large tetragonal distortion. As a result, a temperature-induced tetragonal-to-cubic phase transition occurs, accompanied by a significant NTE effect. This discovery opens up a new avenue for controlling the thermal expansion properties of $PbVO_3$-based perovskites. However, the current understanding of this phenomenon is still in its infancy. More in-depth research is needed to fully explore the effects of different anion substitutions on the NTE property and to elucidate the underlying mechanisms. For example, the interaction between the substituted anions and the cations, as well as how these interactions affect the electronic structure and lattice dynamics of the material, remains to be fully understood.

Despite the significant progress in achieving NTE in metastable $PbVO_3$ through chemical substitutions at the A, B, and anion O sites, several challenges remain in this advanced field. Currently, most NTE in $PbVO_3$-based perovskites are confined to a limited temperature window. This constraint limits their practical applications, especially because numerous real-world applications necessitate materials that exhibit NTE across a broad temperature range. For example, in aerospace applications, materials need to maintain their thermal expansion properties across a large range of temperatures, from the extreme cold of space to the high temperatures experienced during re-entry into the Earth's atmosphere. Therefore, extending the NTE temperature range of $PbVO_3$-based NTE materials is a crucial area for future research. This could involve exploring more complex substitution strategies, such as multi-element co-substitutions or creating composite materials with tailored thermal expansion properties.

i. Although F substitution has been proven to be an effective method for realizing NTE in $PbVO_3$-based perovskites, the study of anion-modified thermal expansion properties is still in its early stages. There is a lack of comprehensive research on the effects of different anion substitutions on the NTE property. Future studies should focus on exploring a wider range of anions, such as Cl^-, Br^-, and S^{2-}, and investigating how their size, electronegativity, and valence state influence the thermal expansion behavior.

ii. Additionally, the fundamental processes behind how anion substitutions result in NTE require deeper exploration. This could involve utilizing sophisticated spectroscopic methods, such as X-ray absorption spectroscopy (XAS) and Raman spectroscopy, to investigate the local structure and vibrational modes of the materials. XAS is a technique that relies on the interaction of X-rays with specific elements in a sample, leading to electron transitions and the emission of X-rays with specific wavelengths. These X-rays carry crucial information about the atomic structure and electronic states of the sample. Raman spectroscopy, on the other hand, is based on the Raman scattering effect, where the interaction of laser light with the sample molecules results in scattered light that reveals the molecular vibrational, rotational, and other low-frequency modes of the material.

iii. Although NTE was achieved in $PbVO_3$-based deviratives by electron-doping, most of these NTE compounds show strong hysteresis, which is not favorable for practical applications. Further investigations are still necessary to solve this problem, in order to improve the NTE performance.

In conclusion, NTE can be realized in $PbVO_3$-based perovskites by destabilizing their large tetragonal distortion via chemical substitutions at the A/B-site cations or the O anion site. These findings have opened up a new path for designing novel NTE materials based on giant tetragonal perovskite materials. Polar perovskites, such as $BiCoO_3$, $Bi(Zn_{1/2}Ti_{1/2})O_3$, and $Bi(Zn_{1/2}V_{1/1})O_3$, which have similar large tetragonal structures to $PbVO_3$, hold great potential for exhibiting NTE if their metastable tetragonal structures can be stabilized. As the quest for new NTE materials continues, the integration of interdisciplinary

approaches combining materials science, chemistry, and physics will be crucial in advancing our understanding of thermal expansion phenomena and unlocking new possibilities for innovative applications. The future of NTE research is of great promise, facilitating the creation of materials that satisfy the rigorous requirements of contemporary engineering and technology. Future research in this area is expected to not only deepen our understanding of the fundamental mechanisms of NTE but also lead to the development of new materials with enhanced thermal expansion properties for a wide range of applications.

Author Contributions

Zhao Pan: writing – original draft, investigation, writing – review and editing, funding acquisition. **Takumi Nishikubo:** formal analysis, writing – review and editing. **Hajime Yamamoto:** formal analysis, writing – review and editing. **Xubin Ye:** formal analysis, writing – review and editing. **Masaki Azuma:** writing – review and editing, funding acquisition. **Youwen Long:** writing – review and editing, funding acquisition.

Acknowledgments

This work was partially supported by the National Natural Science Foundation of China (Nos. 22271309, 12425403, 11921004, and 12261131499), the National Key R&D Program of China (2021YFA1400300), the Grants-in-Aid for Scientific Research (Nos. JP18H05208, JP19H05625, JP24K17509, and JP24H00374) from the Japan Society for the Promotion of Science (JSPS), JSTCREST (No. JPMJCR22O1), and the Kanagawa Institute of Industrial Science and Technology.

Conflicts of Interest

The authors declare no conflicts of interest.

Data Availability Statement

Data sharing is not applicable to this article as no datasets were generated or analyzed during the current study.

References

1. J. S. O. Evans, "Negative Thermal Expansion Materials," *Journal of the Chemical Society Dalton Transactions* 19 (1999): 3317–3326, https://doi.org/10.1039/A904297K.

2. G. D. Barrera, J. A. O. Bruno, T. H. K. Barron, and N. L. Allan, "Negative Thermal Expansion," *Journal of Physics: Condensed Matter* 17, no. 4 (2005): R217–R252, https://doi.org/10.1088/0953-8984/17/4/R03.

3. K. Takenaka, "Negative Thermal Expansion Materials: Technological Key for Control of Thermal Expansion," *Science and Technology of Advanced Materials* 13, no. 1 (2012): 013001, https://doi.org/10.1088/1468-6996/13/1/013001.

4. J. P. Attfield, "Mechanism and Materials for NTE," *Frontiers in Chemistry* 6 (2018): 371, https://doi.org/10.3389/fchem.2018.00371.

5. J. Chen, L. Hu, J. X. Deng, and X. R. Xing, "Negative Thermal Expansion in Functional Materials: Controllable Thermal Expansion by Chemical Modifications," *Chemical Society Review* 44, no. 11 (2015): 3522–3567, https://doi.org/10.1039/C4CS00461B.

6. C. S. Coates and A. L. Goodwin, "How to Quantify Isotropic Negative Thermal Expansion: Magnitude, Range, or Both?," *Materials Horizons* 6, no. 2 (2019): 211–218, https://doi.org/10.1039/C8MH01065J.

7. K. Takenaka, "Progress of Research in Negative Thermal Expansion Materials: Paradigm Shift in the Control of Thermal Expansion," *Frontiers in Chemistry* 6 (2018): 267, https://doi.org/10.3389/fchem.2018.00267.

8. R. Mittal, M. K. Gupt, and S. L. Chaplot, "Phonons and Anomalous Thermal Expansion Behaviour in Crystalline Solids," *Progress in Materials Science* 92 (2018): 360–445, https://doi.org/10.1016/j.pmatsci.2017.10.002.

9. N. X. Burtch, S. J. Baxter, J. Heinen, et al., "Negative Thermal Expansion Design Strategies in a Diverse Series of Metal–Organic Frameworks," *Advanced Functional Materials* 29, no. 48 (2019): 1904669, https://doi.org/10.1002/adfm.201904669.

10. N. K. Shi, Y. Z. Song, X. R. Xing, and J. Chen, "Negative Thermal Expansion in Framework Structure Materials," *Coordination Chemistry Reviews* 449 (2021): 214204, https://doi.org/10.1016/j.ccr.2021.214204.

11. Y. Z. Song, N. K. Shi, S. Q. Deng, X. R. Xing, and J. Chen, "Negative Thermal Expansion in Magnetic Materials," *Progress in Materials Science* 121 (2021): 100835, https://doi.org/10.1016/j.pmatsci.2021.100835.

12. C. Lind, "Two Decades of Negative Thermal Expansion Research: Where Do We Stand?," *Materials* 5, no. 6 (2012): 1125–1154, https://doi.org/10.3390/ma5061125.

13. P. Mohn, "A Century of Zero Expansion," *Nature* 400, no. 6739 (1999): 18–19, https://doi.org/10.1038/21778.

14. K. Scheel, "Versuche ueber die ausdehnung fester koerper, insbesondere von quarz in richtung der hauptachse, platin, palladium und quarzglas bei der temperatur der fluessigen Luft," *Verhandlungen der Deutschen Physikalischen Gesellschaft* 9 (1907): 3–23.

15. K. Scheel, "Ueber die ausdehnung des quarzglases," *Verhandlungen der Deutschen Physikalischen Gesellschaft* 9 (1907): 719–721.

16. F. A. Hummel, "Thermal Expansion Properties of Natural Lithia Minerals," *Foote Prints* 20, no. 2 (1948): 3–11.

17. F. A. Hummel, "Termal Expansion Properties of Some Synthetic Lithia Minerals," *Journal of the American Ceramic Society* 34, no. 8 (1951): 235–239, https://doi.org/10.1111/j.1151-2916.1951.tb11646.x.

18. J. P. Boilot, J. P. Salanie, G. Desplanches, and D. Le Potier, "Phase Transformation in $Na_{1+x}Si_xZr_2P_{3-x}O_{12}$ Compounds," *Materials Research Bulletin* 14, no. 11 (1979): 1469–1477, https://doi.org/10.1016/0025-5408(79)90091-6.

19. S. Y. Limaye, D. K. Agrawal, R. Roy, and Y. Mehrotra, "Synthesis, Sintering and Thermal-Expansion of $Ca_{1-x}Sr_xZr_4P_6O_{24}$-An Ultra-Low Thermal-Expansion Ceramic System," *Journal of Materials Science* 26, no. 1 (1991): 93–98, https://doi.org/10.1007/BF00576037.

20. G. E. Lenain, H. A. McKinstry, J. Alamo, and D. K. Agrawal, "Structural Model for Thermal Expansion in $MZr_2P_3O_{12}$ (M = Li, Na, K, Rb, Cs)," *Journal of Materials Science* 22, no. 1 (1987): 17–22, https://doi.org/10.1007/BF01160546.

21. T. A. Mary, J. S. O. Evans, T. Vogt, and A. W. Sleigh, "Negative Thermal Expansion From 0.3 to 1050 Kelvin in ZrW_2O_8," *Science* 272, no. 5258 (1996): 90–92, https://doi.org/10.1126/science.272.5258.90.

22. Q. Li, K. Lin, Z. N. Liu, et al., "Chemical Diversity for Tailoring Negative Thermal Expansion," *Chemical Reviews* 122, no. 9 (2022): 8438–8486, https://doi.org/10.1021/acs.chemrev.1c00756.

23. X. R. Xing, J. X. Deng, J. Chen, and G. R. Liu, "Novel Thermal Expansion of Lead Titanate," *Rare Metals* 22, no. 4 (2003): 294–297.

24. G. Shirane and S. Hoshino, "On the Phase Transition of Lead Titanate," *Journal of the Physical Society of Japan* 6, no. 4 (1951): 265–270, https://doi.org/10.1143/JPSJ.6.265.

25. B. A. Hunter, B. J. Kennedy, and T. Vogt, "Magnetostriction in a Simple Trivalent Manganese Perovskite," *Physical Review B* 69, no. 2 (2004): 020410, https://doi.org/10.1103/PhysRevB.69.020410.

26. B. K. Greve, K. L. Martin, P. L. Lee, P. J. Chupas, K. W. Chapman, and A. P. Wilkinson, "Pronounced Negative Thermal Expansion From a Simple Structure: Cubic ScF_3," *Journal of the American Chemical Society* 132, no. 44 (2010): 15496–15498, https://doi.org/10.1021/ja106711v.

27. K. Takenaka and H. Takagi, "Giant Negative Thermal Expansion in Ge-Doped Anti-Perovskite Manganese Nitrides," *Applied Physics Letters* 87, no. 26 (2005): 261902, https://doi.org/10.1063/1.2147726.

28. A. L. Goodwin, M. Calleja, M. J. Conterio, et al., "Colossal Positive and Negative Thermal Expansion in the Framework Material $Ag_3[Co(CN)_6]$," *Science* 319, no. 5864 (2008): 794–797, https://doi.org/10.1126/science.115144.

29. N. Shi, Q. L. Gao, A. Sanson, et al., "Negative Thermal Expansion in Cubic $FeFe(CN)_6$ Prussian Blue Analogues," *Dalton Transactions* 48, no. 11 (2019): 3658–3663, https://doi.org/10.1039/c8dt05111a.

30. Q. L. Gao, J. Chen, Q. Sun, et al., "Switching Between Giant Positive and Negative Thermal Expansions of a $YFe(CN)_6$-Based Prussian Blue Analogue Induced by Guest Species," *Angewandte Chemie International Edition* 56, no. 31 (2017): 9023–9028, https://doi.org/10.1002/anie.201702955.

31. Q. L. Gao, J. Q. Wang, A. Sanson, et al., "Discovering Large Isotropic Negative Thermal Expansion in Framework Compound $AgB(CN)_4$ via the Concept of Average Atomic Volume," *Journal of the American Chemical Society* 142, no. 15 (2020): 6935–6939, https://doi.org/10.1021/jacs.0c02188.

32. Q. L. Gao, N. K. Shi, Q. Sun, et al., "Low-Frequency Phonon Driven Negative Thermal Expansion in Cubic $GaFe(CN)_6$ Prussian Blue Analogues," *Inorganic Chemistry* 57, no. 17 (2018): 10918–10924, https://doi.org/10.1021/acs.inorgchem.8b01526.

33. Z. N. Liu, Q. L. Gao, J. Chen, J. Deng, K. Lin, and X. Xing, "Negative Thermal Expansion in Molecular Materials," *Chemical Communications* 54, no. 41 (2018): 5164–5176, https://doi.org/10.1039/C8CC01153B.

34. Z. N. Liu, R. Ma, J. X. Deng, J. Chen, and X. Xing, "Molecular Packing-Dependent Thermal Expansion Behaviors in Metal Squarate Frameworks," *Chemistry of Materials* 32, no. 7 (2020): 2893–2898, https://doi.org/10.1021/acs.chemmater.9b04981.

35. L. Hu, J. Chen, J. Xu, et al., "Atomic Linkage Flexibility Tuned Isotropic Negative, Zero, and Positive Thermal Expansion in $MZrF_6$ (M = Ca, Mn, Fe, Co, Ni, and Zn)," *Journal of the American Chemical Society* 138, no. 44 (2016): 14530–14533, https://doi.org/10.1021/jacs.6b08746.

36. L. Hu, F. Y. Qin, A. Sanson, et al., "Localized Symmetry Breaking for Tuning Thermal Expansion in ScF_3 Nanoscale Frameworks," *Journal of the American Chemical Society* 140, no. 13 (2018): 4477–4480, https://doi.org/10.1021/jacs.8b00885.

37. F. Han, J. Chen, L. Hu, et al., "The Distortion-Adjusted Change of Thermal Expansion Behavior of Cubic Magnetic Semiconductor $(Sc_{1-x}M_x)F_3$ (M = Al, Fe)," *Journal of the American Ceramic Society* 99, no. 9 (2016): 2886–2888, https://doi.org/10.1111/jace.14399.

38. T. Wang, J. L. Xu, L. Hu, et al., "Tunable Thermal Expansion and Magnetism in Zr-Doped ScF_3," *Applied Physics Letters* 109, no. 18 (2016): 181901, https://doi.org/10.1063/1.4966958.

39. F. Y. Qin, J. Chen, U. Aydemir, et al., "Isotropic Zero Thermal Expansion and Local Vibrational Dynamics in $(Sc, Fe)F_3$," *Inorganic Chemistry* 56, no. 18 (2017): 10840–10843, https://doi.org/10.1021/acs.inorgchem.7b01234.

40. Q. L. Gao, N. K. Shi, A. Sanson, et al., "Tunable Thermal Expansion From Negative, Zero, to Positive in Cubic Prussian Blue Analogues of $GaFe(CN)_6$," *Inorganic Chemistry* 57, no. 22 (2018): 14027–14030, https://doi.org/10.1021/acs.inorgchem.8b02428.

41. Q. L. Gao, Y. Sun, N. K. Shi, et al., "Large Isotropic Negative Thermal Expansion in Water-Free Prussian Blue Analogues of $ScCo(CN)_6$," *Scripta Materialia* 187 (2020): 119–124, https://doi.org/10.1016/j.scriptamat.2020.05.041.

42. Q. L. Gao, Y. X. Jiao, Q. Sun, et al., "Giant Negative Thermal Expansion in Ultralight $NaB(CN)_4$," *Angewandte Chemie International Edition* 136, no. 13 (2024): e202401302, https://doi.org/10.1002/anie.202401302.

43. Q. L. Gao, S. Zhang, Y. X. Jiao, et al., "A New Isotropic Negative Thermal Expansion Material of $CaSnF_6$ With Facil and Low-Cost Synthesis," *Nano Research* 16, no. 4 (2023): 5964–5972, https://doi.org/10.1007/s12274-022-5288-0.

44. H. Zhao, Y. Q. Qiao, K. Y. Zhao, et al., "Negative Thermal Expansion in $ABC(MoO_4)_3$ Compounds," *Small* 20, no. 42 (2024): 2403000, https://doi.org/10.1002/smll.202403000.

45. J. Q. Wang, Q. L. Gao, Y. X. Gao, et al., "Uniaxial Negative Thermal Expansion Behavior of β-CuSCN," *Applied Physics Letters* 118, no. 22 (2021): 22210, https://doi.org/10.1063/5.0051596.

46. Y. Q. Liu, D. J. Mei, N. Z. Wang, M. S. Molokeev, X. Jiang, and Z. Lin, "Intrinsic Isotropic Near-Zero Thermal Expansion in $Zn_4B_6O_{12}X$ (X = O, S, Se)," *ACS Applied Materials & Interfaces* 12, no. 34 (2020): 38435–38440, https://doi.org/10.1021/acsami.0c12351.

47. X. X. Jiang, M. S. Molokeev, L. Y. Dong, et al., "Anomalous Mechanical Materials Squeezing Three-Dimensional Volume Compressibility Into One Dimension," *Nature Communications* 11, no. 1 (2020): 5593, https://doi.org/10.1038/s41467-020-19219-5.

48. X. Y. Song, Z. H. Sun, Q. Z. Huang, et al., "Adjustable Zero Thermal Expansion in Antiperovskite Mangnese Nitride," *Advanced Materials* 23, no. 40 (2011): 4690–4694, https://doi.org/10.1002/ADMA.201102552.

49. K. Takenaka, T. Inagaki, and H. Takagi, "Conversion of Magnetic Structure by Slight Dopants in Geometrically Frustrated Antiperovskite Mn_3GaN," *Applied Physics Letters* 95, no. 13 (2009): 132508, https://doi.org/10.1063/1.3243340.

50. R. J. Huang, L. F. Li, F. S. Cai, X. D. Xu, and L. H. Qian, "Low-temperature Negative Thermal Expansion of the Antiperovskite Manganses Nitride Mn_3CuN Codoped With Ge and Si," *Applied Physics Letters* 93, no. 8 (2008): 081902, https://doi.org/10.1063/1.2970998.

51. K. Kodama, S. Iikubo, K. Takenaka, M. Takigawa, H. Takagi, and S. Shamoto, "Gradual Development of Γ^{5g} Antiferromagnetic Moment in the Giant Negative Thermal Expansion Material $Mn_3Cu_{1-x}Ge_xN$ ($x \sim 0.5$)," *Physical Review B* 81, no. 22 (2010): 224419, https://doi.org/10.1103/PhysRevB.81.224419.

52. P. Tong, D. Louca, G. King, A. Llobet, J. Lin, and Y. Sun, "Magnetic Transition Broadening and Local Lattice Distortion in the Negative Thermal Expansion Antiperovskite $Cu_{1-x}Sn_xNMn_3$," *Applied Physics Letters* 102, no. 4 (2013): 041908, https://doi.org/10.1063/1.4790151.

53. J. C. Lin, B. S. Wang, S. Lin, et al., "The Study of Negative Thermal Expansion and Magnetic Evolution in Antiperovskite Compounds $Cu_{0.8-x}Sn_xMn_{0.2}NMn_3$ ($0 \leq X \leq 0.3$)," *Journal of Applied Physics* 111, no. 4 (2012): 043905, https://doi.org/10.1063/1.3684653.

54. Y. Sun, C. Wang, Y. C. Wen, et al., "Negative Thermal Expansion and Magnetic Transition in Anti-Perovskite Structured $Mn_3Zn_{1-x}Sn_xN$ Compounds," *Journal of the American Ceramic Society* 93, no. 8 (2010): 2178–2181, https://doi.org/10.1111/j.1551-2916.2010.03711.x.

55. X. L. Yuan, B. Wang, Y. Sun, et al., "High-Entropy Anti-Perovskites With Enhanced Negative Thermal Expansion Behavior," *Advanced Functional Materials* 34, no. 42 (2024): 2404629, https://doi.org/10.1002/adfm.202404629.

56. K. Lin, W. J. Li, C. Y. Yu, et al., "High Performance and Low Thermal Expansion in Er-Fe-V-Mo Dual-Phase Alloys," *Acta Materialia* 198, no. 1 (2020): 271–280, https://doi.org/10.1016/j.actamat.2020.08.012.

57. C. Y. Yu, K. Lin, Q. H. Zhang, et al., "An Isotropic Zero Thermal Expansion Alloy With Super-High Toughness," *Nature Communications* 15, no. 1 (2024): 2252, https://doi.org/10.1038/s41467-024-46613-0.

58. Y. L. Cao, H. W. Zhou, S. Khmelevskyi, et al., "Pressure-Modulated Magnetism and Negative Thermal Expansion in the Ho_2Fe_{17} Intermetallic Compound," *Chemistry of Materials* 35, no. 8 (2023): 3249–3255, https://doi.org/10.1021/acs.chemmater.3c00158.

59. Y. L. Cao, K. Lin, S. Khmelevskyi, et al., "Ultrawide Temperature Range Super-Invar Behavior of $R_2(Fe,Co)_{17}$ Materials (R = Rare Earth)," *Physical Review Letters* 127, no. 5 (2021): 055501, https://doi.org/10.1103/PhysRevLett.127.055501.

60. Y. Z. Song, Q. Sun, M. Xu, et al., "Negative Thermal Expansion in (Sc, Ti)Fe_2 Induced by an Unconventional Magnetovolume Effect," *Materials Horizons* 7, no. 1 (2020): 275–281, https://doi.org/10.1039/C9MH01025D.

61. J. C. He, Z. Pan, D. Su, et al., "Magnetic-Field-Induced Sign Changes of Thermal Expansion in $DyCrO_4$," *Chinese Physics Letters* 40, no. 6 (2023): 066501, https://doi.org/10.1088/0256-307X/40/6/066501.

62. Y. W. Long, N. Hayashi, T. Saito, M. Azuma, S. Muranaka, and Y. Shimakawa, "Temperature-Induced A-B Intersite Charge Transfer in an A-Site-Odered $LaCu_3Fe_4O_{12}$ Perovskite," *Nature* 458, no. 7234 (2009): 60–63, https://doi.org/10.1038/nature07816.

63. M. Azuma, W. T. Chen, H. Seki, et al., "Colossal Negative Thermal Expansion in $BiNiO_3$ Induced by Intermetallic Charge Transfer," *Nature Communications* 2, no. 1 (2011): 347, https://doi.org/10.1038/ncomms1361.

64. I. Yamada, K. Tsuchida, K. Ohgushi, et al., "Giant Negative Thermal Expansion in the Iron Perovskite $SrCu_3Fe_4O_{12}$," *Angewandte Chemie International Edition* 50, no. 29 (2011): 6579–6582, https://doi.org/10.1002/anie.201102228.

65. I. Yamada, S. Marukawa, M. MuraKami, and S. Mori, "True" Negative Thermal Expansion in Mn-Doped $LaCu_3Fe_4O_{12}$ Perovskite Oxides," *Applied Physics Letters* 105, no. 23 (2014): 231906, https://doi.org/10.1063/1.4903890.

66. D. Asai, Y. Mizuno, H. Hasegawa, et al., "Valence Fluctuations and Giant Isotropic Negative Thermal Expansion in $Sm_{1-x}R_xS$ (R = Y, La, Ce, Pr, Nd)," *Applied Physics Letters* 114, no. 14 (2019): 141902, https://doi.org/10.1063/1.5090546.

67. M. Braden, G. Andre, S. Nakatsuji, and Y. Maeno, "Crystal and Magnetic Structure of Ca_2RuO_4: Magnetoelastic Coupling and the Metal-Insulator Transition," *Physical Review B* 58, no. 2 (1998): 847–861, https://doi.org/10.1103/PhysRevB.58.847.

68. T. F. Qi, O. B. Korneta, S. Parkin, L. E. De Long, P. Schlottmann, and G. Cao, "Negative Volume Thermal Expansion via Orbital and Magnetic Orders in $Ca_2Ru_{1-x}Cr_xO_4$ ($0 < X < 0.13$)," *Physical Review Letters* 105, no. 17 (2010): 177203, https://doi.org/10.1103/PhysRevLett.105.177203.

69. T. F. Qi, O. B. Korneta, S. Parkin, J. Hu, and G. Cao, "Magnetic and Orbital Orders Coupled to Negative Thermal Expansion in Mott Insulators $Ca_2Ru_{1-x}M_xO_4$ (M = Mn and Fe)," *Physical Review B* 85, no. 16 (2012): 165143, https://doi.org/10.1103/PhysRevB.85.165143.

70. J. Chen, F. F. Wang, Q. Z. Huang, et al., "Effectively Control Negative Thermal Expansion of Single-Phase Ferroelectrics of $PbTiO_3$-(Bi,La)FeO_3 Over a Giant Range," *Scientific Report* 3, no. 1 (2013): 2458, https://doi.org/10.1038/srep02458.

71. T. Yang, K. Lin, N. Wang, et al., "Tunable Thermal Expansion and High Hardness of (0.9-x)$PbTiO_3$-$x$$CaTiO_3$-0.1Bi$(Zn_{2/3}Ta_{1/3})O_3$ Ceramics," *Inorganic Chemistry Frontiers* 6, no. 4 (2019): 1068–1072, https://doi.org/10.1039/C9QI00087A.

72. T. Yang, K. Lin, Q. Li, et al., "Evidence of the Enhanced Negative Thermal Expansion in (1-x)$PbTiO_3$-xBi$(Zn_{2/3}Ta_{1/3})O_3$," *Inorganic Chemistry Frontiers* 7, no. 5 (2020): 1284–1288, https://doi.org/10.1039/C9QI01694E.

73. T. Yang, Y. L. Wang, L. L. Fan, et al., "Strong Covalent Bonding for Enhanced Negative Thermal Expansion in (1-x)$PbTiO_3$-$x$$BiGaO_3$," *Journal of Physical Chemistry C* 124, no. 37 (2020): 20445–20449, https://doi.org/10.1021/acs.jpcc.0c05948.

74. Z. Pan, J. Chen, X. X. Jiang, et al., "Enhanced Tetragonality and Large Negative Thermal Expansion in a New Pb/Bi-Based Perovskite Ferroelectric of (1-x)$PbTiO_3$-xBi$(Zn_{1/2}V_{1/1})O_3$," *Inorganic Chemistry Frontiers* 6, no. 8 (2019): 1990–1995, https://doi.org/10.1039/C9QI00450E.

75. Y. Sakai, K. Matsuno, T. Nishikubo, et al., "Two Types of Negative Thermal Expansion Observed in $PbCr_{1-x}Ti_xO_3$," *Chemistry of Materials* 35, no. 3 (2023): 1008–1015, https://doi.org/10.1021/acs.chemmater.2c02896.

76. H. T. Zhao, Z. Pan, X. Shen, et al., "Antiferroelectricity-Induced Negative Thermal Expansion in Double Perovskite Pb_2CoMoO_6," *Small* 20, no. 2 (2024): 2305219, https://doi.org/10.1002/smll.202305219.

77. Y. C. Rong, M. L. Li, J. Chen, et al., "Large Negative Thermal Expansion in Non-Perovskite Lead-Free Ferroelectric $Sn_2P_2S_6$," *Physical Chemistry Chemical Physics* 18, no. 8 (2016): 6247–6251, https://doi.org/10.1039/C6CP00011H.

78. Y. C. Rong, K. Lin, F. M. Guo, et al., "Tailoring Negative Thermal Expansion in Ferroelectric $Sn_2P_2S_6$ by Lone-Pair Cations," *Journal of Physical Chemistry C* 121, no. 3 (2017): 1832–1837, https://doi.org/10.1021/acs.jpcc.6b09146.

79. Z. Pan, X. X. Jiang, R. Z. Yu, et al., "Transformation of Thermal Expansion From Large Volume Contraction to Nonlinear Strong NegativeThermal Expansion in $PbTiO_3$-Bi$(Co_{1-x}Fe_x)O_3$ Perovskites," *ACS Materials & Interfaces* 14, no. 20 (2022): 23610–23616, https://doi.org/10.1021/acsami.2c00771.

80. Z. Pan, F. Y. Zhou, M. Q. Ye, et al., "Realizing Negative Thermal Expansion Over an Extended Temperature Range in $PbTiO_3$-Based Perovskites," *Journal of Advanced Ceramics* 14, no. 7 (2025): 9221096, https://doi.org/10.26599/JAC.2025.9221096.

81. Z. Pan, Y.-W. Fang, S. A. Nikolaev, et al., "Anion-Mediated Unusual Enhancement of Negative Thermal Expansion in the Oxyfluoride of $PbTiO_3$," *Materials Horizons* 12, no. 17 (2025): 6804–6811, https://doi.org/10.1039/d5mh00251f.

82. Z. Pan, X. X. Jiang, T. Nishikubo, et al., "Pronounced Negative Thermal Expansion in Lead-Free $BiCoO_3$-Based Ferroelectrics Triggered by the Stabilized Perovskite Structure," *Chemistry of Materials* 31, no. 16 (2019): 6187–6192, https://doi.org/10.1021/acs.chemmater.9b01969.

83. H. Ishizaki, Y. Sakai, T. Nishikubo, et al., "Negative Thermal Expansion in Lead-Free La-Substituted $Bi_{0.5}Na_{0.5}VO_3$," *Chemistry of Materials* 32, no. 11 (2020): 4832–4837, https://doi.org/10.1021/acs.chemmater.0c01709.

84. Z. Pan, T. Koike, T. Nishikubo, et al., "Realization of Negative Thermal Expansion in Lead-Free $Bi_{0.5}K_{0.5}VO_3$ by the Suppression of Tetragonality," *Inorganic Chemistry* 61, no. 8 (2021): 3730–3735, https://doi.org/10.1021/acs.inorgchem.1c03960.

85. T. Nishikubo, T. Ogata, L. K. Venkataraman, et al., "Polarization- and Strain-Mediated Control of Negative Thermal Expansion and Ferroelasticity in $BiInO_3$–$BiZn_{1/2}Ti_{1/2}O_3$," *Chemistry of Materials* 33, no. 4 (2021): 1498–1505, https://doi.org/10.1021/acs.chemmater.0c04049.

86. T. Nishikubo, T. Imai, Y. Sakai, et al., "Polar-Nonpolar Transition-Type Negative Thermal Expansion With 11.1% Volume Shrinkage by Design," *Chemistry of Materials* 35, no. 3 (2023): 870–878, https://doi.org/10.1021/acs.chemmater.2c02304.

87. J. Chen, X. R. Xing, R. B. Yu, and G. R. Liu, "Thermal Expansion Properties of Lanthanum-Substituted Lead Titanate Ceramics," *Journal of the American Ceramic Society* 88, no. 5 (2005): 1356–1358, https://doi.org/10.1111/j.1551-2916.2005.00314.x.

88. X. R. Xing, J. X. Deng, Z. Q. Zhu, and G. R. Liu, "Soilid Solution $Ba_{1-x}Pb_xTiO_3$ and Its Thermal Expansion," *Journal of Alloys and Compounds* 353, no. 1–2 (2023): 1–4, https://doi.org/10.1016/S0925-8388(02)01178-7.

89. X. R. Xing, J. Chen, J. X. Deng, and G. R. Liu, "Soilid Solution $Pb_{1-x}Sr_xTiO_3$ and Its Thermal Expansion," *Journal of Alloys and Compounds* 360, no. 1–2 (2023): 286–289, https://doi.org/10.1016/S0925-8388(03)00345-1.

90. J. Chen, X. R. Xing, R. B. Yu, and G. R. Liu, "Structure and Enhancement of Negative Thermal Expansion in the $PbTiO_3$-$CdTiO_3$ System," *Applied Physics Letters* 87, no. 23 (2005): 231915, https://doi.org/10.1063/1.2140486.

91. P. H. Hu, Z. M. Cao, J. Chen, et al., "Structure and Negative Thermal Expansion of $Pb_{1-x}Bi_xTiO_3$," *Materials Letters* 62, no. 30 (2008): 4585–4587, https://doi.org/10.1016/j.matlet.2008.08.028.

92. C. Sun, Z. M. Cao, J. Chen, et al., "Negative Thermal Expansion in the $PbTi_{1-x}Fe_xO_3$ System," *Physica Status Solidi B* 245, no. 11 (2008): 2520–2523, https://doi.org/10.1002/pssb.200880265.

93. Z. Pan, J. Chen, X. X. Jiang, et al., "Colossal Volume Contraction in Strong Polar Perovskite of Pb(Ti, V)O_3," *Journal of the American Chemical Society* 139, no. 42 (2017): 14865–14868, https://doi.org/10.1021/jacs.7b08625.

94. P. H. Hu, J. Chen, J. X. Deng, and X. R. Xing, "Thermal Expansion, Ferroelectric and Magnetic Properties in $(1-x)PbTiO_3$-$xBi(Ni_{1/2}Ti_{1/2})O_3$," *Journal of the American Chemical Society* 132, no. 6 (2010): 1925–1928, https://doi.org/10.1021/ja908014u.

95. Z. Pan, J. Chen, R. Z. Yu, et al., "Large Negative Thermal Expansion Induced by Synergistic Effects of Ferroelectrostriction and Spin Crossover in $PbTiO_3$-Based Perovskites," *Chemistry of Materials* 31, no. 4 (2019): 1296–1303, https://doi.org/10.1021/acs.chemmater.8b04266.

96. Z. Pan, Y. W. Fang, T. Nishikubo, L. Hu, S. Kawaguchi, and M. Azuma, "Tolerance Factor Control of Tetragonality and Negative Thermal Expansionin $PbTiO_3$-Based Ferroelectrics," *Chemistry of Materials* 34, no. 6 (2022): 2798–2803, https://doi.org/10.1021/acs.chemmater.2c00076.

97. Z. Pan, S. A. Nikolaev, J. Zhang, et al., "Extend the Scope of Negative Thermal Expansion in $PbTiO_3$-Based Perovskites," *Applied Physics Letters* 126, no. 7 (2025): 071901, https://doi.org/10.1063/5.0253686.

98. Z. Pan, Z. L. Liang, X. Wang, et al., "Mixed Anion Control of Enhanced Negative Thermal Expansion in the Oxysulfide of $PbTiO_3$," *Materials Horizons* 11, no. 21 (2024): 5394–5401, https://doi.org/10.1039/D4MH00795F.

99. J. Chen, X. R. Xing, J. X. Deng, and G. R. Liu, "Thermal Expansion of Ceramics in the System $Pb_{1-x}(La_{1/2}K_{1/1})TiO_3$," *Journal of Alloys and Compounds* 372, no. 1–2 (2004): 259–266, https://doi.org/10.1016/j.jallcom.2003.09.137.

100. P. H. Hu, J. Chen, X. Y. Sun, et al., "Zero Thermal Expansion in $(1-x)PbTiO_3$-$xBi(Mg,Ti)_{1/2}O_3$ Piezoceramics," *Journal of Materials Chemistry* 19, no. 11 (2009): 1648–1652, https://doi.org/10.1039/B816822A.

101. J. Chen, X. R. Xing, G. R. Liu, J. H. Li, and Y. T. Liu, "Structure and Negative Thermal Expansion in the $PbTiO_3$-$BiFeO_3$ System," *Applied Physics Letters* 89, no. 10 (2006): 101914, https://doi.org/10.1063/1.2347279.

102. Z. Pan, M. Q. Ye, Y. Suo, et al., "Achieving Negative Thermal Expansion Over an Extended Temperature Range in Rare Earth-Modified $PbTiO_3$-Based Perovskites," *Rare Metals* 44, no. 9 (2025): 6494–6502, https://doi.org/10.1007/s12598-025-03310-1.

103. J. Chen, X. R. Xing, C. Sun, et al., "Zero Thermal Expansion in $PbTiO_3$-Based Perovskites," *Journal of the American Chemical Society* 130, no. 4 (2008): 1144–1145, https://doi.org/10.1021/ja7100278.

104. Z. Pan, J. Chen, X. X. Jiang, et al., "Zero Thermal Expansion and Semiconducting Properties in $PbTiO_3$-Bi(Co, Ti)O_3 Ferroelectric Solid Solutions," *Inorganic Chemistry* 56, no. 5 (2017): 2589–2595, https://doi.org/10.1021/acs.inorgchem.6b02761.

105. R. V. Shapnchenko, V. V. Chernaya, A. A. Tsirlin, et al., "Synthesis, Structure, and Properties of New Perovskite $PbVO_3$," *Chemistry of Materials* 16, no. 17 (2004): 3267–3273, https://doi.org/10.1021/cm049310x.

106. A. A. Belik, M. Azuma, T. Saito, Y. Shimakawa, and M. Takano, "Crystallographic Features and Tetragonal Phase Stability of $PbVO_3$, a New Member of $PbTiO_3$ Family," *Chemistry of Materials* 17, no. 2 (2005): 269–273, https://doi.org/10.1021/cm048387i.

107. R. Z. Yu, H. Hojo, K. Oka, et al., "New $PbTiO_3$-Type Giant Tetragonal Compound Bi_2ZnVO_6 and Its Stability Under Pressure," *Chemistry of Materials* 27, no. 6 (2015): 2012–2017, https://doi.org/10.1021/cm504133e.

108. Z. Pan, T. Nishikubo, Y. Sakai, T. Yamamoto, S. Kawaguchi, and M. Azuma, "Observation of Stabilized Monoclinic Phase as a 'Bridge' at the Morphotropic Phase Boundary Between Tetragonal Perovskite $PbVO_3$ and Rhombohedral $BiFeO_3$," *Chemistry of Materials* 32, no. 8 (2020): 3615–3620, https://doi.org/10.1021/acs.chemmater.0c00944.

109. K. Oka, I. Yamada, M. Azuma, et al., "Magnetic Ground-State of Perovskite $PbVO_3$ With Large Tetragonal Distortion," *Inorganic Chemistry* 47, no. 16 (2008): 7355–7359, https://doi.org/10.1021/ic800649a.

110. A. A. Belik, T. Yamauchi, H. Ueda, et al., "Absence of Metallic Conductivity in Tetragonal and Cubic $PbVO_3$ at High Pressure," *Journal of the Physical Society of Japan* 83, no. 7 (2014): 074711, https://doi.org/10.7566/JPSJ.83.074711.

111. H. Yamamoto, T. Imai, Y. Sakai, and M. Azuma, "Colossal Negative Thermal Expansion in Electron-Doped $PbVO_3$ Perovskites," *Angewandte Chemie International Edition* 57, no. 27 (2018): 8170–8173, https://doi.org/10.1002/anie.201804082.

112. T. Ogata, Y. Sakai, H. Yamamoto, et al., "Melting of D_{xy} Orbital Ordering Accompanied by Suppression of Giant Tetragonal Distortion and Insulator-to-Metal Transition in Cr Substituted $PbVO_3$," *Chemistry of Materials* 31, no. 4 (2019): 1352–1358, https://doi.org/10.1021/acs.chemmater.8b04680.

113. G. Q. Xi, Z. Pan, Y. W. Fang, et al., "Anion-Induced Robust Ferroelectricity in Sulfurized Pseudo-Rhombohedral Epitaxial $BiFeO_3$ Thin Films via Polarization Rotation," *Materials Horizons* 10, no. 10 (2023): 4389–4397, https://doi.org/10.1039/D3MH00716B.

114. K. Oka, T. Ichibha, D. Kato, et al., "Anionic Ordering in $Pb_2Ti_4O_9F_2$ Revisited by Nuclear Magnetic Resonance and Density Functional Theory," *Dalton Transactions* 51, no. 40 (2022): 15361–15369, https://doi.org/10.1039/D2DT00839D.

115. T. Ogata, K. Oka, and M. Azuma, "Negative Thermal Expansion in Electron Doped $PbVO_{3-x}F_x$," *Applied Physics Express* 12, no. 2 (2019): 023005, https://doi.org/10.7567/1882-0786/aafb9b.